

Stone monuments of the Nemrud Dag sanctuary/Turkey – petrographical investigation and diagnosis of weathering damage

Kurt Heinrichs & Bernd Fitzner*

Heinrichs, K. & Fitzner, B. (2007): Stone monuments of the Nemrud Dag sanctuary/Turkey – petrographical investigation and diagnosis of weathering damage. [Steinmonumente des Nemrud Dag Heiligtums/Türkei – petrographische Untersuchung und Diagnose der Verwitterungsschäden.] – Z. dt. Ges. Geowiss., 158: 519–548 Stuttgart.

Abstract: The sanctuary of the Nemrud Dag in Eastern Turkey represents outstanding world cultural heritage. It was built by King Antiochos I of Commagene in the first century B.C. It is composed of a tumulus and three terraces. The west and east terrace are famous for their colossal limestone statues and sandstone stelae. These stone monuments have suffered weathering damage. The awareness of increasing damage and the danger of further irretrievable loss of cultural heritage have resulted in international efforts for sustainable monument preservation. Studies have been carried out, targeted to damage diagnosis as a fundamental contribution to appropriate monument preservation. The investigation has so far focused on the sandstone monuments and combines laboratory analysis of representative stone samples and in-situ investigation of the weathering damage by means of monument mapping and ultrasonic measurements. Field work was conducted in 1988 and 2002. Results are presented for the sandstone monuments regarding petrographical properties, state of weathering, rating of weathering damage and weathering progression. In addition, preliminary results are presented for the limestone monuments. The findings reveal a considerable petrographical range of the sandstones. The extent of damage on the sandstone monuments and weathering prognoses derived from evaluation of weathering damage indicate the need and urgency of monument preservation measures.

Kurzfassung: Die Kultstätte des Nemrud Dag in der Osttürkei gehört zum Weltkulturerbe. Sie wurde von König Antiochos I. von Kommagene im ersten Jahrhundert vor Christus errichtet. Die Anlage besteht aus einem Tumulus (Grabhügel) und drei Terrassen. Auf der Westterrasse und der Ostterrasse befinden sich mächtige Kalksteinstatuen und Reliefstelen aus Sandstein. Diese Steinmonumente haben erhebliche Verwitterungsschäden erlitten. Die Zunahme der Schäden und die daraus erwachsende Gefahr weiteren Verlustes von kulturellem Erbe haben internationale Bemühungen um dauerhaft wirksame Erhaltungsmaßnahmen ausgelöst. An den Steinmonumenten wurden Untersuchungen zur Schadensdiagnose als Grundlage für die Planung und Durchführung geeigneter Schutzmaßnahmen durchgeführt. Die Untersuchungen konzentrierten sich bisher auf die Monumente aus Sandstein. Sie umfassten petrographische Laboruntersuchungen an repräsentativen Gesteinsproben sowie Vor-Ort-Untersuchungen der Verwitterungsschäden mit Hilfe der Bauwerkskartierung und Ultraschallmessungen. Geländekampagnen wurden in den Jahren 1988 und 2002 durchgeführt. Petrographische Eigenschaften, Verwitterungszustand, Schadensbewertung und Verwitterungsfortschritt werden für die Sandsteinmonumente ausführlich beschrieben und diskutiert. Zusätzlich werden erste Ergebnisse für die Kalksteinstatuen vorgestellt. Die Ergebnisse zeigen eine erhebliche petrographische Bandbreite der Sandsteine. Die Sandsteinmonumente sind insbesondere von Gesteinsverlust und Gesteinsablösungen unterschiedlicher Art und oft hoher Intensität betroffen. Schadensklassen und Schadensindizes haben sich als aussagekräftige Parameter für die Schadensbewertung erwiesen. Hohe Anteile starker bis sehr starker Schäden und hohe Schadensindizes weisen auf einen Besorgnis erregenden Zustand der meisten Sandsteinmonumente hin. Die Ergebnisse zur Verwitterungsprogression – abgeleitet aus den vergleichenden Studien in den Jahren 1988 und 2002 und Auswertungen von fotografischem Archivmaterial – lassen eine beachtliche Zunahme der Verwitterungsschäden innerhalb der letzten einhundert Jahre erkennen. Dies führt zu alarmierenden Schadensprognosen. Die Untersuchungsergebnisse verdeutlichen die Notwendigkeit und Dringlichkeit von Erhaltungsmaßnahmen.

* Addresses of the authors:

Dr. Kurt Heinrichs, Department of Engineering Geology and Hydrogeology, RWTH Aachen University, Lochnerstraße 4–20, D-52064 Aachen, Germany (heinrichs@lih.rwth-aachen.de);

Dr. Bernd Fitzner, Geological Institute, RWTH Aachen University, Working group “Natural stones and weathering”, Wuellnerstraße 2, D-52062 Aachen, Germany (fitzner@geol.rwth-aachen.de).

Keywords: Nemrud Dag, stone monuments, sandstone, limestone, stone weathering, damage diagnosis, petrographical studies, monument mapping, ultrasonic measurements, damage categories, damage index, weathering progression

Schlüsselwörter: Nemrud Dag, Steinmonumente, Sandstein, Kalkstein, Gesteinsverwitterung, Schadensdiagnose, petrographische Untersuchung, Bauwerkskartierung, Ultraschallmessungen, Schadensklassen, Schadensindex, Verwitterungsprogression

1. Introduction

The sanctuary of Nemrud Dag is located on the top of Mount Nemrut (2150 m) in Eastern Turkey near the village of Karadut in the Adiyaman Province (Fig. 1). The sanctuary represents the most prominent masterpiece of Commagene culture. The Kingdom of Commagene was founded by Mithridates I. At its height the Commagene Kingdom north of Syria extended to the Toros Mountains in the north and to the Euphrates River in the east. Kings of the Commagene Dynasty ruled the Adiyaman Province and its vicinity from 80 B.C. until 72 A.D. The sanctuary of Nemrud Dag was built by King Antiochos I, son of Mithridates I. King Antiochos I ruled from 69 to 36 B.C. The sanctuary was rediscovered by the German engineer Karl Sester in 1881. It is of very high historical, archaeological, technological, religious, and tourism significance. It was added to UNESCO's World Heritage List in 1987. The sanctuary is composed of a tumulus and three terraces – west, east, and north. The tumulus – thought to cover the royal tomb – is made of coarse crushed limestone. Its original height of 75 m has decreased over time to 50 m. The east terrace and west terraces show a similar composition, originally including one row of colossal limestone statues (Antiochos I, Commagene, Zeus, Apollo, Herakles, two guardian eagles, and lions) up to 10 m in height and three rows of sandstone stelae/sculptures forming an open courtyard (stelae with dexiosis reliefs showing the King shaking hands with Commagene, Apollo, Zeus, and Herakles; stela with the Lion Horoscope; stelae with reliefs of the Persian and Macedonian ancestors of Antiochos I; guardian eagles and lions). On the northern terrace only unfinished sandstone stelae are found. The limestone statues are composed of huge limestone blocks (whitish, massive limestone); each of the sandstone stelae was made from one sandstone block only. The exact origin of the limestones and sandstones is not known.

K. Humann, O. Puchstein, O. Hamdi Bey, Th. Goell, F.K. Dörner, R. Naumann, H. Hauptmann, and S. Sahin can be considered as pioneers of archaeological and conservation work on Nemrud Dag (e.g. Humann & Puchstein 1890, Doerner 1987, Sanders 1996). For some years, the International Nemrud Foundation (INF) has been involved in research and conservation activities at the site.

The current situation of the stone monuments is alarming (Figs. 2–5). All stone monuments have suffered

damage from weathering. Moreover, all limestone statues and most of the sandstone stelae have fallen. Some objects (esp. heads of the limestone statues and some sandstone stelae) have been partly re-erected where they were lying. Most of the sandstone stelae on the east terrace are lost.

The studies presented in this paper started in 1988. In this year a first field campaign was carried out at Nemrud Dag aimed at diagnosis of stone materials and weathering damage on the stone monuments (Fitzner & Düppenbecker 1991). Information and documents obtained from these first studies were compiled as the basis of a second, more extensive field campaign in 2002. The 2002 field campaign was carried out on behalf of the World Monuments Fund (WMF). The field studies concentrated on the sandstone monuments, in addition preliminary studies on the limestone statues were made (Fitzner et al. 2003). The investigation of the sandstone monuments comprised lithological survey, mapping of weathering forms and ultrasonic measurements. Based on in-situ studies of the sandstones according to macroscopic criteria, representative samples for petrographical analysis were collected with the permission of the Turkish authorities. The results presented for the sandstone monuments address petrographical properties (mineral composition, textural properties, porosity properties, hygric properties, petrophysical properties), state of weathering (type, intensity, and combination of weathering forms, ultrasonic velocities), extent of weathering damage (damage categories, damage indices) and weathering progression (extent of damage as function of time).

2. Petrographical properties

On four limestone samples (L 1–L 4) preliminary petrographical studies were carried out. Twenty-six representative – unweathered and weathered – sandstone samples (S 1–S 26) were studied in detail with respect to mineral composition, textural properties, porosity properties, hygric properties, and petrophysical properties. The samples were prepared for the individual measuring procedures (powder samples, thin sections, drill cores, cubes). Laboratory analysis included X-ray diffraction, transmitted light microscopy with image analysis, scanning electron microscopy (SEM), mercury porosimetry, nitrogen sorption procedure (BET-method), various standardized



Fig. 1



Fig. 2



Fig. 3



Fig. 4



Fig. 5

Fig. 1: Mount Nemrut with the sanctuary of Nemrud Dag on its top.

Fig. 2: Nemrud Dag – west terrace.

Fig. 3: Nemrud Dag – east terrace.

Fig. 4: Zeus dexiosis stele – west terrace, sandstone.

Fig. 5: Head of the Antiochos I statue – west terrace, limestone.

water adsorption/desorption tests, ultrasonic measurements, and drilling resistance measurements.

2.1. Limestones

The whitish, hard limestones can be characterized as pure limestones (Tab. 1). The calcite ($\geq 99.9\%$) occurs in these limestones as sparite (62–86%), micrite (14–33%) and bioclasts (1–4%). Subordinately, the limestones may contain clay minerals ($\leq 0.1\%$). Bedding structures can not be observed. Networks of coarsely sparitic veins are characteristic for the limestones. The total porosity of the limestones amounts to about 1 vol.-%. Micropores (pores with radii $\leq 0.1\ \mu\text{m}$) are prevalent. The pore surface ranges between 0.04 and 0.1 m^2/g , respectively between 0.1 and 0.3 m^2/cm^3 . Ultrasonic velocities range between 4000 and 5000 m/s.

2.2. Sandstones

The sandstones – greenish to greyish in colour (Munsell Rock-Colour Chart: HUE 5Y 6/1, light olive grey) – show a considerable range in terms of their mineral composition (Tab. 2, Figs. 6, 7). They consist of quartz (5–15%), feldspar (8–26% / albite, microcline), rock fragments (14–38% / fragments of sedimentary, magmatic, and metamorphic rocks), chlorite (less than 4%), mica (less than 3% / biotite, muscovite, glauconite), heavy minerals (less than 1% / zircon, tourmaline, rutile) and matrix (carbonatic matrix: 23–41% / mainly calcite, rarely dolomite; non-carbonatic matrix: 6–24% / clay minerals, opaque matter, finest quartz). The ratio of carbonatic matrix to non-carbonatic matrix ranges between 1.3 and 6.2. According to Pettijohn et al. (1987) the sandstones are to be classified as “lithic greywacke” (exception: sample S 24 – “feldspathic greywacke”).

The grain/matrix ratio ranges between 0.8 and 2.4 (Tab. 3). With increasing grain/matrix ratio, the ratio of rock fragments to quartz and feldspar tends to increase

Tab. 1: Mineral composition – limestones. Transmitted light microscopy.

| Sample | Mineral composition (%) | | | |
|--------|-------------------------|---------|-----------|---------------|
| | Calcite | | | Clay minerals |
| | Sparite | Micrite | Bioclasts | |
| L 1 | 62.1 | 33.4 | 4.4 | 0.1 |
| L 2 | 86.0 | 13.6 | 0.4 | – |
| L 3 | 79.3 | 20.0 | 0.6 | 0.1 |
| L 4 | 86.3 | 13.5 | 0.1 | 0.1 |

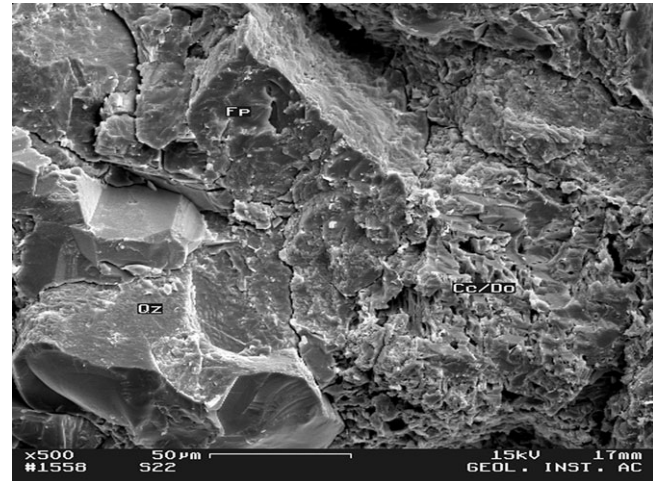


Fig. 6: Mineral composition – sandstone. SEM-micrograph, image width: ~ 0.23 mm. Qz = quartz, Fp = feldspar, Cc = calcite, Do = dolomite.

(0.5–1.6). The sandstones show a mainly matrix-supported fabric, direct grain contacts (point contacts) are rather rare. All sandstones show parallel bedding indicated by compositional and grain size variation.

With respect to grain size analysis, only components $> 30\ \mu\text{m}$ were considered as grains according to Pettijohn et al. (1987). As shown in table 3, the mean grain size increases from quartz (0.15–0.24 mm, very fine sand – fine sand according to the Wentworth classification) via feldspar (0.17–0.30 mm, fine sand – medium sand) to the rock fragments (0.22–0.51 mm, fine sand – coarse sand). Considering all grains, the mean grain size of the sandstones ranges between 0.19 and 0.32 mm (fine sand – medium sand). The mean grain size of the sandstone tends to

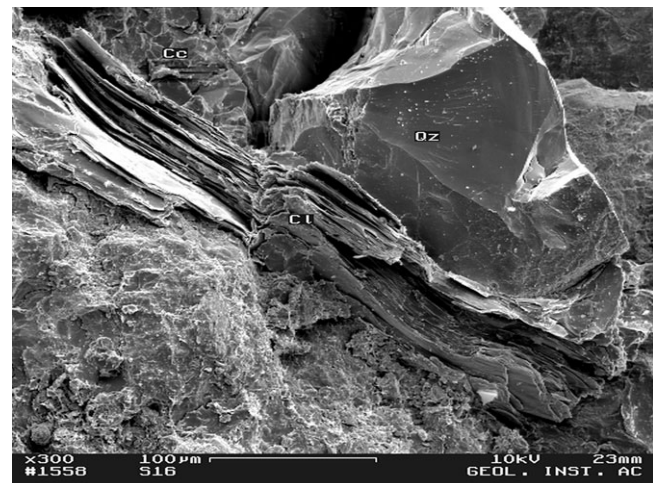


Fig. 7: Mineral composition – sandstone. SEM-micrograph, image width: ~ 0.39 mm. Qz = quartz, Cc = calcite, Cl = chlorite.

Tab. 2: Mineral composition – sandstones. X-ray diffraction, transmitted light microscopy.

| Sample | Mineral composition (%) | | | | | | | |
|----------------|--|-----------------------|-----------------------------|----------|-------------------|-----------------------------|---|------------------------------------|
| | Grains (components > 30 μm) ¹ | | | | | | Matrix (components \leq 30 μm) ¹ | |
| | Quartz | Feldspar ² | Rock fragments ³ | Chlorite | Mica ⁴ | Heavy minerals ⁵ | Carbonatic matrix ⁶ | Non-carbonatic matrix ⁷ |
| S 1 | 10.8 | 16.8 | 23.2 | 2.3 | 0.4 | 0.1 | 32.6 | 13.8 |
| S 2 | 11.0 | 20.0 | 25.2 | 1.4 | 0.3 | 0.1 | 29.4 | 12.6 |
| S 3 | 11.5 | 14.4 | 31.1 | 1.1 | 0.2 | 0.1 | 30.3 | 11.3 |
| S 4 | 5.3 | 20.2 | 21.8 | 1.1 | 0.4 | + | 37.6 | 13.6 |
| S 5 | 9.5 | 17.9 | 24.0 | 0.8 | 0.6 | 0.1 | 33.8 | 13.3 |
| S 6 | 7.8 | 15.7 | 19.4 | 1.2 | 0.5 | 0.1 | 35.1 | 20.2 |
| S 7 | 15.4 | 8.0 | 25.4 | 1.9 | 1.8 | + | 40.9 | 6.6 |
| S 8 | 14.0 | 11.6 | 37.7 | 1.4 | 0.5 | 0.1 | 26.7 | 8.0 |
| S 9 | 13.6 | 18.4 | 19.1 | 1.7 | 0.9 | + | 29.8 | 16.5 |
| S 10 | 13.8 | 18.2 | 26.0 | 2.8 | 0.6 | + | 24.9 | 13.7 |
| S 11 | 7.8 | 16.8 | 24.0 | 1.9 | 0.5 | + | 41.4 | 7.6 |
| S 12 | 11.2 | 21.7 | 29.6 | 1.1 | 0.2 | + | 27.8 | 8.4 |
| S 13 | 10.3 | 25.5 | 27.1 | 1.1 | 0.7 | + | 27.5 | 7.8 |
| S 14 | 11.8 | 9.2 | 27.4 | 3.6 | 2.4 | + | 35.7 | 9.9 |
| S 15 | 11.0 | 23.6 | 24.0 | 1.6 | 0.4 | + | 23.0 | 16.4 |
| S 16 | 9.8 | 21.0 | 25.5 | 1.8 | 0.4 | + | 26.3 | 15.2 |
| S 17 | 9.0 | 18.0 | 34.1 | 1.4 | 0.4 | + | 31.1 | 6.0 |
| S 18 | 7.6 | 22.6 | 37.9 | 2.0 | 0.4 | + | 23.9 | 5.6 |
| S 19 | 10.4 | 23.5 | 24.1 | 1.0 | 0.2 | + | 24.7 | 16.1 |
| S 20 | 12.0 | 14.8 | 21.6 | 1.2 | 0.4 | + | 36.0 | 14.0 |
| S 21 | 10.9 | 14.8 | 24.9 | 1.1 | 0.1 | + | 32.1 | 16.1 |
| S 22 | 6.9 | 11.6 | 29.0 | 1.3 | 0.1 | 0.1 | 29.9 | 21.1 |
| S 23 | 9.5 | 12.3 | 22.5 | 0.9 | 0.6 | 0.2 | 40.5 | 13.5 |
| S 24 | 11.1 | 16.6 | 13.7 | 1.5 | 0.3 | 0.3 | 32.4 | 24.1 |
| S 25 | 10.6 | 16.5 | 17.8 | 0.9 | 0.2 | 0.1 | 36.8 | 17.1 |
| S 26 | 9.3 | 13.0 | 24.0 | 2.0 | 0.2 | 0.2 | 32.9 | 18.4 |
| Minimum | 5.3 | 8.0 | 13.7 | 0.8 | 0.1 | + | 23.0 | 5.6 |
| Maximum | 15.4 | 25.5 | 37.9 | 3.6 | 2.4 | 0.3 | 41.4 | 24.1 |

¹ size limits according to Pettijohn et al. (1987); ² albite, microcline; ³ fragments of sedimentary, magmatic and metamorphic rocks; ⁴ biotite, muscovite, glauconite; ⁵ zircon, tourmaline, rutile, + = content < 0.1%; ⁶ mainly calcite, subordinately dolomite; ⁷ clay minerals (chlorite, illite, mica), opaque matter (eg. hematite), finest quartz

increase with increasing grain/matrix ratio. Most of the sandstones show a moderate sorting of their grains. Increasing mean grain size of the sandstones tends to correlate with slight decreasing degree of sorting. The grain size distribution of the sandstones is presented in table 4. According to the Wentworth classification, grain sizes of the sandstones range from coarse silt (0.03125–0.0625

mm) to granule (2–4 mm). However, not all sandstones have grains in the classes of “very coarse sand” and “granule”. The sandstones have the main proportion of grains (63–83 %) in the classes “fine sand” (0.125–0.25 mm) and “medium sand” (0.25–0.5 mm).

Table 5 shows the porosity properties of the sandstones that were studied by means of mercury porosime-

Tab. 3: Grain/matrix ratio and grain size characteristics – sandstones. Transmitted light microscopy with image analysis.

| Sample | Grain-matrix-ratio | Grain size characteristics ¹ | | | | | | |
|----------------|--------------------|---|----------|----------------|------------|--|-------------------------|----------|
| | | Mean grain size M (mm) ² | | | | | Sorting So ⁴ | |
| | | Quartz | Feldspar | Rock fragments | All grains | Classification according to Wentworth ³ | All grains | |
| S 1 | 1.16 | 0.23 | 0.29 | 0.44 | 0.30 | medium sand | 1.51 | moderate |
| S 2 | 1.38 | 0.21 | 0.26 | 0.42 | 0.28 | medium sand | 1.59 | moderate |
| S 3 | 1.40 | 0.24 | 0.28 | 0.51 | 0.32 | medium sand | 1.61 | moderate |
| S 4 | 0.95 | 0.17 | 0.23 | 0.34 | 0.26 | medium sand | 1.58 | moderate |
| S 5 | 1.12 | 0.18 | 0.22 | 0.32 | 0.25 | fine sand | 1.54 | moderate |
| S 6 | 0.81 | 0.16 | 0.21 | 0.33 | 0.22 | fine sand | 1.53 | moderate |
| S 7 | 1.11 | 0.16 | 0.21 | 0.30 | 0.20 | fine sand | 1.63 | moderate |
| S 8 | 1.88 | 0.18 | 0.25 | 0.40 | 0.28 | medium sand | 1.64 | moderate |
| S 9 | 1.16 | 0.16 | 0.22 | 0.33 | 0.22 | fine sand | 1.56 | moderate |
| S 10 | 1.59 | 0.19 | 0.25 | 0.38 | 0.26 | medium sand | 1.61 | moderate |
| S 11 | 1.04 | 0.15 | 0.17 | 0.26 | 0.19 | fine sand | 1.53 | moderate |
| S 12 | 1.76 | 0.17 | 0.25 | 0.43 | 0.26 | medium sand | 1.69 | moderate |
| S 13 | 1.83 | 0.18 | 0.22 | 0.34 | 0.24 | fine sand | 1.59 | moderate |
| S 14 | 1.19 | 0.23 | 0.27 | 0.22 | 0.24 | fine sand | 1.46 | moderate |
| S 15 | 1.54 | 0.18 | 0.22 | 0.34 | 0.23 | fine sand | 1.54 | moderate |
| S 16 | 1.41 | 0.19 | 0.24 | 0.38 | 0.25 | fine sand | 1.69 | moderate |
| S 17 | 1.70 | 0.18 | 0.23 | 0.35 | 0.26 | medium sand | 1.60 | moderate |
| S 18 | 2.39 | 0.19 | 0.24 | 0.39 | 0.28 | medium sand | 1.66 | moderate |
| S 19 | 1.45 | 0.17 | 0.24 | 0.39 | 0.25 | fine sand | 1.66 | moderate |
| S 20 | 1.00 | 0.16 | 0.23 | 0.25 | 0.22 | fine sand | 1.53 | moderate |
| S 21 | 1.07 | 0.20 | 0.30 | 0.45 | 0.29 | medium sand | 1.57 | moderate |
| S 22 | 0.96 | 0.17 | 0.28 | 0.46 | 0.27 | medium sand | 1.66 | moderate |
| S 23 | 0.85 | 0.23 | 0.28 | 0.48 | 0.29 | medium sand | 1.54 | moderate |
| S 24 | 0.77 | 0.16 | 0.21 | 0.35 | 0.20 | fine sand | 1.51 | moderate |
| S 25 | 0.86 | 0.17 | 0.22 | 0.30 | 0.21 | fine sand | 1.40 | good |
| S 26 | 0.95 | 0.19 | 0.27 | 0.34 | 0.26 | medium sand | 1.50 | moderate |
| Minimum | 0.77 | 0.15 | 0.17 | 0.22 | 0.19 | fine sand | 1.40 | good |
| Maximum | 2.39 | 0.24 | 0.30 | 0.51 | 0.32 | medium sand | 1.69 | moderate |

¹ Grains = components > 30 μm (according to Pettijohn et al. 1987);

² mean grain size M according to Trask (in Tucker 1988) $M = \frac{P_{25} + P_{75}}{2}$;

³ Wentworth, 1922 (in Pettijohn et al. 1987), considering the mean grain size of all grains;

⁴ sorting So according to Trask (in Tucker 1988) $So = \sqrt{\frac{P_{75}}{P_{25}}}$, 1.00 – 1.23 very well sorted, 1.23 – 1.41 well sorted, 1.41 – 1.74 moderately sorted, 1.74 – 2.00 poorly sorted, > 2.0 very poorly sorted

Tab. 4: Grain size distribution – sandstones. Transmitted light microscopy with image analysis.

| Sample | Grain size distribution (% of grains) ¹ | | | | | | |
|----------------|--|------------------|----------------|--------------|-------------|------------------|--------------|
| | 0.03125 –0.0625 mm | 0.0625 –0.125 mm | 0.125 –0.25 mm | 0.25 –0.5 mm | 0.5 –1 mm | 1 –2 mm | 2 –4 mm |
| | Coarse silt | Very fine sand | Fine sand | Medium sand | Coarse sand | Very coarse sand | Granule sand |
| S 1 | 0.6 | 7.9 | 34.1 | 41.1 | 15.2 | 1.1 | – |
| S 2 | 1.9 | 12.6 | 35.4 | 34.2 | 13.8 | 2.1 | – |
| S 3 | 0.7 | 9.8 | 30.4 | 37.3 | 17.1 | 3.6 | 1.1 |
| S 4 | 1.4 | 16.6 | 36.2 | 38.8 | 5.9 | 1.1 | – |
| S 5 | 2.2 | 15.3 | 42.9 | 33.6 | 5.7 | 0.3 | – |
| S 6 | 3.1 | 18.8 | 42.4 | 30.1 | 5.1 | 0.5 | – |
| S 7 | 10.0 | 21.7 | 47.5 | 18.0 | 2.6 | 0.2 | – |
| S 8 | 4.0 | 13.4 | 33.6 | 31.4 | 13.3 | 2.9 | 1.4 |
| S 9 | 5.6 | 18.5 | 40.2 | 28.1 | 7.1 | 0.5 | – |
| S 10 | 5.5 | 15.5 | 33.7 | 34.0 | 9.7 | 1.6 | – |
| S 11 | 5.9 | 22.9 | 43.2 | 24.9 | 2.6 | 0.3 | 0.2 |
| S 12 | 6.7 | 15.5 | 31.1 | 31.9 | 12.5 | 2.3 | – |
| S 13 | 3.8 | 17.4 | 36.9 | 31.4 | 8.2 | 1.7 | 0.6 |
| S 14 | 1.9 | 12.0 | 45.5 | 37.4 | 3.2 | – | – |
| S 15 | 4.2 | 15.4 | 41.3 | 30.8 | 7.1 | 1.2 | – |
| S 16 | 6.8 | 17.5 | 30.6 | 33.4 | 9.1 | 2.0 | 0.6 |
| S 17 | 3.5 | 14.7 | 34.7 | 34.7 | 11.6 | 0.8 | – |
| S 18 | 4.6 | 13.8 | 29.2 | 35.0 | 12.7 | 4.4 | 0.3 |
| S 19 | 5.3 | 18.4 | 33.8 | 29.8 | 11.3 | 1.4 | – |
| S 20 | 5.7 | 16.3 | 41.8 | 31.0 | 4.4 | 0.8 | – |
| S 21 | 3.4 | 10.7 | 30.2 | 39.6 | 14.1 | 2.0 | – |
| S 22 | 3.7 | 15.8 | 33.5 | 30.6 | 14.3 | 2.1 | – |
| S 23 | 2.2 | 10.2 | 30.4 | 42.0 | 13.1 | 2.1 | – |
| S 24 | 2.3 | 23.2 | 44.1 | 25.5 | 4.1 | 0.8 | – |
| S 25 | 2.1 | 15.5 | 50.5 | 28.7 | 3.2 | – | – |
| S 26 | 1.8 | 12.1 | 36.3 | 41.3 | 7.2 | 1.0 | 0.3 |
| Minimum | 0.6 | 7.9 | 29.2 | 18.0 | 2.6 | – | – |
| Maximum | 10.0 | 23.2 | 50.5 | 42.0 | 17.1 | 4.4 | 1.4 |

¹ grain size classes according to Wentworth (1922) in Pettijohn et al. (1987), only grains (components > 30 μm) considered, matrix (components \leq 30 μm – clay to medium silt) not considered

try and nitrogen sorption procedure (BET-method). The density of the sandstones ranges between 2.67 and 2.73 g/cm³, the bulk density of the unweathered samples between 2.46 and 2.56 g/cm³. The unweathered sandstones are characterized by low total porosity (5.2–8.8 vol.-%). Capillary pores (pores with radii > 0.1 μm) are prevailing (3.1–7.0 vol.-%). The proportion of micropores in the unweathered sandstones (pores with radii 0.1 μm) ranges between

1.4 and 2.1 vol.-%. The results obtained from mercury porosimetry show somewhat elevated figures for total porosity and portion of capillary pores due to the measuring procedure (here ~ 1 vol.-% on average too high, as the comparison with porosities calculated from water immersion tests at pressure shows; Tab. 6). The sandstones show very small median radii of pore entries (0.04–0.34 μm). The pore surface of the unweathered sandstones can be

Tab. 5: Porosity properties – sandstones. Mercury porosimetry, nitrogen sorption procedure (BET-method).

| Sample | Bulk density g / cm ³ | Density g / cm ³ | Total porosity vol.-% | Micropores (r ≤ 0.1 μm) vol.-% | Capillary pores (r > 0.1 μm) vol.-% | Median radius of pore entries μm | Pore surface m ² / g | Pore surface m ² / cm ³ |
|----------------|-------------------------------------|--------------------------------|--------------------------|--------------------------------------|---|--|------------------------------------|--|
| S 1 | 2.52 | 2.70 | 6.47 | 1.85 | 4.62 | 0.10 | 3.73 | 9.41 |
| S 2 | 2.53 | 2.68 | 5.68 | 1.60 | 4.08 | 0.11 | 3.24 | 8.21 |
| S 3 | 2.49 | 2.69 | 7.61 | 2.06 | 5.55 | 0.12 | 4.04 | 10.04 |
| S 4 | 2.52 | 2.67 | 5.62 | 1.76 | 3.86 | 0.05 | 4.12 | 10.37 |
| S 5 | 2.55 | 2.69 | 5.42 | 1.73 | 3.69 | 0.08 | 3.74 | 9.52 |
| S 6 | 2.56 | 2.70 | 5.20 | 2.06 | 3.14 | 0.05 | 4.59 | 11.73 |
| S 7 | 2.53 | 2.69 | 5.94 | 2.04 | 3.90 | 0.05 | 4.37 | 11.07 |
| S 8 | 2.49 | 2.70 | 7.79 | 1.98 | 5.81 | 0.17 | 4.24 | 10.55 |
| S 9 | 2.46 | 2.69 | 8.68 | 1.77 | 6.91 | 0.16 | 3.65 | 8.98 |
| S 10 | 2.46 | 2.69 | 8.82 | 1.96 | 6.87 | 0.28 | 4.40 | 10.81 |
| S 11 | 2.53 | 2.70 | 6.42 | 2.02 | 4.40 | 0.11 | 4.77 | 12.05 |
| S 12 | 2.51 | 2.70 | 6.87 | 1.66 | 5.21 | 0.12 | 3.11 | 7.82 |
| S 13 | 2.49 | 2.69 | 7.49 | 1.72 | 5.77 | 0.12 | 3.87 | 9.61 |
| S 14 | 2.53 | 2.69 | 5.84 | 1.60 | 4.24 | 0.11 | 3.13 | 7.93 |
| S 15 | 2.53 | 2.70 | 6.18 | 1.97 | 4.21 | 0.07 | 3.46 | 8.77 |
| S 16 | 2.52 | 2.69 | 6.38 | 1.67 | 4.71 | 0.23 | 2.98 | 7.50 |
| S 17 | 2.48 | 2.69 | 7.94 | 1.60 | 6.34 | 0.20 | 3.10 | 7.68 |
| S 18 * | 2.38 | 2.67 | 10.83 | 1.75 | 9.08 | 0.99 | 3.92 | 9.34 |
| S 19 * | 2.40 | 2.69 | 10.81 | 1.80 | 9.01 | 0.53 | 3.39 | 8.13 |
| S 20 | 2.49 | 2.73 | 8.79 | 1.79 | 7.00 | 0.26 | 3.60 | 8.96 |
| S 21 | 2.54 | 2.69 | 5.56 | 1.62 | 3.94 | 0.04 | 2.84 | 7.21 |
| S 22 | 2.51 | 2.69 | 6.71 | 1.62 | 5.09 | 0.22 | 3.37 | 8.46 |
| S 23 | 2.51 | 2.69 | 6.64 | 1.37 | 5.27 | 0.34 | 3.04 | 7.64 |
| S 24 | 2.50 | 2.71 | 7.73 | 1.68 | 6.05 | 0.13 | 3.14 | 7.84 |
| S 25 | 2.52 | 2.70 | 6.72 | 1.56 | 5.16 | 0.12 | 2.71 | 6.82 |
| S 26 | 2.49 | 2.70 | 7.94 | 1.65 | 6.29 | 0.27 | 3.88 | 9.67 |
| Minimum | 2.46 (2.38 *) | 2.67 | 5.20 | 1.37 | 3.14 | 0.04 | 2.71 | 6.82 |
| Maximum | 2.56 | 2.73 | 8.82 (10.83 *) | 2.06 | 7.00 (9.08 *) | 0.34 (0.99 *) | 4.77 | 12.05 |

* weathered samples (granular disintegration)

considered as rather high (2.7–4.8 m²/g, respectively 6.8–12.1 m²/cm³). With increasing total porosity of the sandstones the proportion of capillary pores, the capillary pores/micropores ratio and the median radius of pore entries tend to increase. The increasing proportion of micropores correlates with increasing pore surface.

The total porosity of the weathered sandstones (those exhibiting surface granular disintegration) is increased

(~ 11 vol.-%), accompanied by increased portion of capillary pores and median radius of pore entries.

Results of the water adsorption behaviour of the sandstones are presented in table 6. Due to the low total porosity of the sandstones, their water uptake is also low. When immersed in water under pressure (150 bar), the water uptake of the unweathered sandstones ranges between 4.3 and 7.8 vol.-%. When immersed in water at at-

Tab. 6: Hygric properties – sandstones. Water adsorption tests – immersion, capillary soaking.

| Sample | Water adsorption | | | | | | |
|----------------|--|--|--|------------------------------|-------------------------------------|--------------------------------|--|
| | Immersion tests | | | Capillary soaking test | | | |
| | Water uptake at atmospheric pressure | Water uptake at pressure (150 bar) | Saturation coefficient ¹ | Water uptake coefficient | Water penetration coefficient | Water capacity ² | Impregnation coefficient ³ |
| vol.-% | vol.-% | – | kg / m ² h ^{0.5} | m / h ^{0.5} | vol.-% | – | |
| S 1 | 4.53 | 4.88 | 0.93 | 0.33 | 0.008 | 4.28 | 0.88 |
| S 2 | 3.88 | 4.25 | 0.91 | 0.25 | 0.007 | 3.64 | 0.86 |
| S 3 | 5.69 | 5.90 | 0.96 | 0.85 | 0.016 | 5.45 | 0.92 |
| S 4 | 4.24 | 4.72 | 0.90 | 0.21 | 0.005 | 3.89 | 0.82 |
| S 5 | 4.25 | 4.67 | 0.91 | 0.43 | 0.011 | 3.98 | 0.85 |
| S 6 | 4.73 | 5.42 | 0.87 | 0.23 | 0.006 | 4.17 | 0.77 |
| S 7 | 4.42 | 4.53 | 0.98 | 0.31 | 0.008 | 4.15 | 0.92 |
| S 8 | 7.39 | 7.62 | 0.97 | no measurements ⁴ | | | |
| S 9 | 6.47 | 6.55 | 0.99 | no measurements ⁴ | | | |
| S 10 | 7.62 | 7.76 | 0.98 | no measurements ⁴ | | | |
| S 11 | 4.05 | 4.54 | 0.89 | 0.19 | 0.005 | 3.68 | 0.81 |
| S 12 | 5.23 | 5.38 | 0.97 | 0.82 | 0.017 | 4.95 | 0.92 |
| S 13 | 6.17 | 6.37 | 0.97 | 1.13 | 0.019 | 5.91 | 0.93 |
| S 14 | 5.47 | 5.54 | 0.99 | no measurements ⁴ | | | |
| S 15 | 4.90 | 5.21 | 0.94 | 0.85 | 0.018 | 4.73 | 0.91 |
| S 16 | 5.71 | 6.00 | 0.95 | 0.78 | 0.014 | 5.39 | 0.90 |
| S 17 | 6.21 | 7.07 | 0.88 | no measurements ⁴ | | | |
| S 18* | 10.00 | 10.19 | 0.98 | no measurements ⁴ | | | |
| S 19* | 10.03 | 10.56 | 0.95 | no measurements ⁴ | | | |
| S 20 | 5.85 | 6.34 | 0.92 | no measurements ⁴ | | | |
| S 21 | 4.87 | 4.96 | 0.98 | 0.49 | 0.012 | 4.07 | 0.82 |
| S 22 | 7.04 | 7.54 | 0.93 | no measurements ⁴ | | | |
| S 23 | 5.01 | 5.28 | 0.95 | no measurements ⁴ | | | |
| S 24 | 6.53 | 7.25 | 0.90 | no measurements ⁴ | | | |
| S 25 | 5.91 | 6.07 | 0.97 | no measurements ⁴ | | | |
| S 26 | 6.62 | 6.90 | 0.96 | no measurements ⁴ | | | |
| Minimum | 3.88 | 4.25 | 0.87 | 0.19 | 0.005 | 3.64 | 0.77 |
| Maximum | 7.62 (10.03 *) | 7.76 (10.56 *) | 0.99 | 1.13 | 0.019 | 5.91 | 0.93 |

¹ saturation coefficient = water uptake at atmospheric pressure (vol.-%) : water uptake at pressure (vol.-%)² water capacity = capillary water uptake (vol.-%)³ impregnation coefficient = water capacity (vol.-%) : water uptake at pressure (vol.-%)⁴ measurements not possible due to the size / shape of the sample

* weathered samples (granular disintegration)

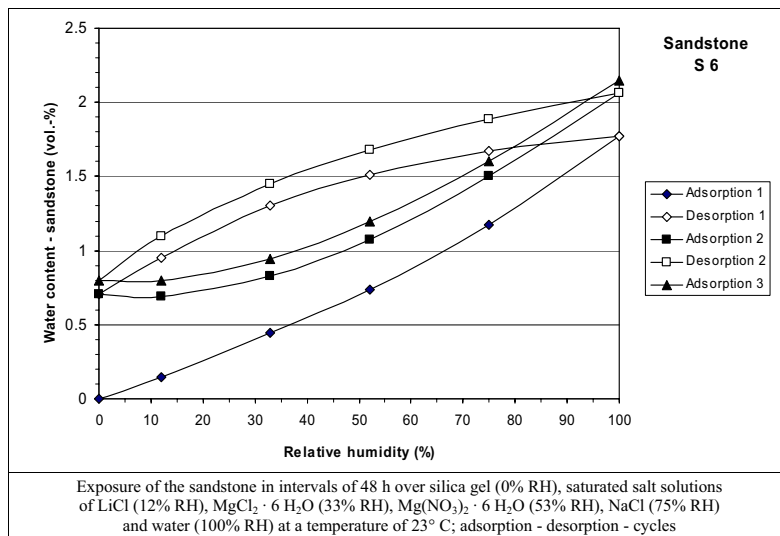


Fig. 8: Isothermal adsorption of air humidity (Sandstone S 6).

atmospheric pressure, their water uptake ranges between 3.9 and 7.86 vol.-%. The unweathered sandstones are characterized by high to very high saturation coefficients (0.87–0.99). With respect to capillary soaking, their water uptake coefficient ranges between 0.2 and 1.1 kg/m²h^{0.5}, their water penetration coefficient between 5 and 20 mm/h^{0.5}, their water capacity between 3.6 and 5.9 vol.-% and their impregnation coefficient between 0.77 and 0.93. Here it has to be noted that not all samples could be studied by means of capillary soaking tests due to their insufficient size. Water uptake of the unweathered sandstones at atmospheric pressure, water uptake at pressure (150 bar), water uptake coefficient, water penetration coefficient, and water capacity tend to increase with increasing total porosity of the sandstones. Water uptake of the weathered sandstones (granular disintegration) is increased.

In addition to water uptake measurements by means of immersion and capillary soaking tests, the isothermal

adsorption of air humidity was measured. Results are presented in figure 8 for the sandstone with S 6 as an example. The adsorption of air humidity is decisively controlled by the portion of micropores and the process of capillary condensation. It was found that the water content of the sandstones – expressed in vol.-% – in the adsorption/desorption cycle test at a temperature of 23 °C approximates to the volume of their micropores at the end of the adsorption phases. Longer exposure of the sandstones at continuously 100 % RH/23 °C results in further increase of water content in the sandstones (additional water content between 0.8 and 1.3 vol.-%, partial filling of capillary pores). This means that the sandstones of Nemrud Dag can be considered as “wet” when exposed over a long period at high air humidity.

A water desorption test was carried out by constant exposure of the sandstones samples after capillary soaking at 23 °C/45 % RH. It was found that they retain a rather high residual humidity. After 48 days the residual

Tab. 7: Petrophysical properties – sandstones. Ultrasonic measurements.

| | | Ultrasonic velocity (m/s) | | | | Anisotropy index (–) ¹ | |
|---------------------|--|---------------------------|---------|--------------------------|---------|-----------------------------------|---------|
| | | Parallel to bedding | | Perpendicular to bedding | | Minimum | Maximum |
| | | Minimum | Maximum | Minimum | Maximum | | |
| Unweathered samples | | 2300 | 3800 | 1800 | 3800 | 1.0 | 1.3 |
| Weathered samples | Splitting along bedding planes (exfoliation) | 2250 | 3750 | 800 | 2200 | 1.5 | 4.5 |
| | Splitting along bedding planes (exfoliation) in combination with granular disintegration | 1400 | 1700 | 700 | 1200 | 1.2 | 2.0 |

¹ anisotropy index = ultrasonic velocity parallel to bedding: ultrasonic velocity perpendicular to bedding

Tab. 8: Tendentious correlations between the petrographical properties of the sandstones.

| | | | |
|--|---|--------|---|
| Grain / matrix ratio | - | —————▶ | + |
| Ratio – rock fragments / quartz + feldspar | - | —————▶ | + |
| Mean grain size | - | —————▶ | + |
| Degree of sorting | + | ◀————— | - |
| Total porosity | - | —————▶ | + |
| Proportion of capillary pores | - | —————▶ | + |
| Capillary pores / micropores ratio | - | —————▶ | + |
| Median radius of pore entries | - | —————▶ | + |
| Water uptake at atmospheric pressure (immersion) | - | —————▶ | + |
| Water uptake at pressure (immersion) | - | —————▶ | + |
| Water uptake coefficient (capillary water uptake) | - | —————▶ | + |
| Water penetration coefficient (capillary water uptake) | - | —————▶ | + |
| Water capacity (capillary water uptake) | - | —————▶ | + |
| Ultrasonic velocity – parallel to bedding | + | ◀————— | - |
| Ultrasonic velocity – perpendicular to bedding | + | ◀————— | - |
| Anisotropy index | - | —————▶ | + |
| Independent of the relations above, following relations can be stated additionally | | | |
| Proportion of micropores | - | —————▶ | + |
| Pore surface | - | —————▶ | + |
| Adsorption of air humidity | - | —————▶ | + |
| Retained residual humidity (water desorption test) | - | —————▶ | + |
| lower – —————▶ + higher | | | |

humidity ranged between 20 and 35 % of the water content after capillary soaking. This corresponds to 1.0–1.5 vol.-% water, respectively, up to 30 % of the open pore space remains filled with water. Higher proportions of micropores in the sandstones correlate with higher residual humidity.

Table 7 shows petrophysical properties of the sandstones. With respect to the unweathered sandstones, ultrasonic velocities parallel to bedding range between 2300 and 3800 m/s, ultrasonic velocities perpendicular to bedding between 1800 and 3800 m/s. The ultrasonic velocities parallel to bedding as well as those perpendicular to bedding tend to decrease with increasing grain/matrix ratio, mean grain size and total porosity of the sandstones. The anisotropy index ranges between 1.0 (no anisotropy) and 1.3 (rather high anisotropy). Tendentiously, it increases with increasing grain/matrix ratio and mean grain size of the sandstones. Results of drilling resistance measurements indicate the high hardness of the sandstones in unweathered condition. The results for the weathered sandstones can be summarized as follows: exfoliation (splitting along bedding plans) results in considerably reduced ultrasonic velocities perpendicular to bed-

ding and intensified anisotropy of the sandstones. Granular disintegration results in a further significant reduction of ultrasonic velocity, both parallel and perpendicular to bedding. Granular disintegration partly compensates for the effects of anisotropy.

The tendentious correlations between the different stone properties of the sandstones are summarized in table 8.

Frost weathering is considered as an important weathering process affecting the Nemrud Dag monuments. Weathering simulation tests (freeze/thaw cycle tests) have shown that the coarser-grained sandstones are more vulnerable to granular disintegration than the finer-grained, less porous sandstones, whereas the finer-grained sandstones are more vulnerable to exfoliation.

3. State of weathering

Preliminary studies on weathering damage to the limestone monuments were made using visual inspection, surface profile measurements and microscope studies. The weathering state of the sandstone monuments was stud-

ied in detail based on the survey, classification, mapping, and evaluation of weathering forms and ultrasonic measurements. Results are presented in terms of type, intensity, and distribution of weathering forms, rating of weathering damage and weathering progression including risk prognosis. Results obtained from monument mapping in 2002 were then compared to those gathered in 1988. In addition, old photographs were evaluated to assess weathering progression over a longer period.

3.1. Limestones

The main weathering phenomena observed on the limestone statues are a loss of compact stone fragments, cracks and especially microkarst (Figs. 9, 10). Microscope studies (transmitted light microscopy, scanning electron microscopy) have shown that microkarstification often originates from physical disintegration of the coarsely sparitic veins in the limestones resulting in an

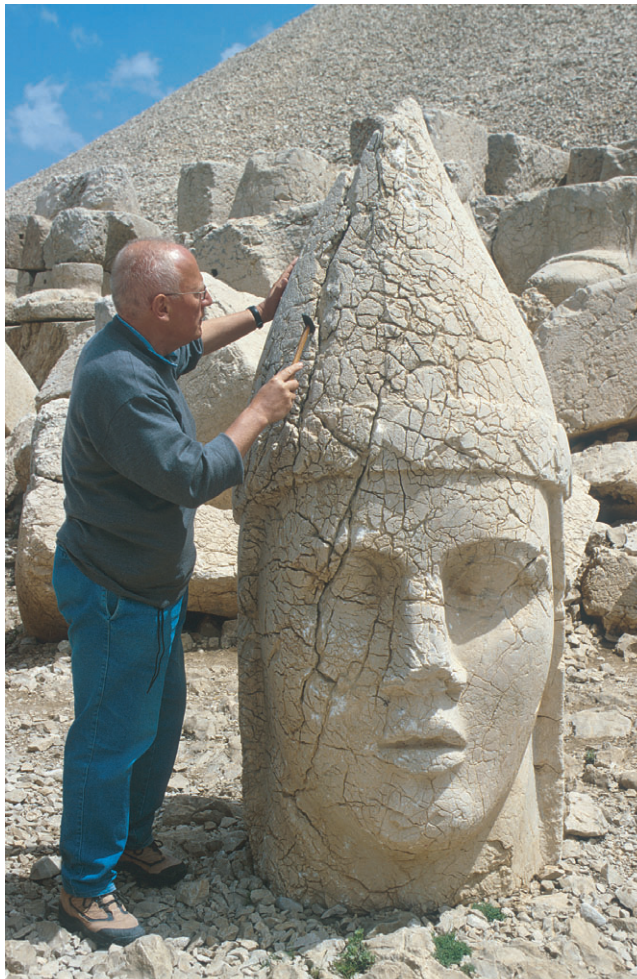


Fig. 9: Head of Apollo – west terrace, limestone. Loss of stone fragments, cracks, and microkarst.



Fig. 10: Microkarst – limestone statue. Width of the section: 24 cm.

increase in porosity (Fig. 11). This intensifies water penetration and related dissolution processes. The microkarst forms extend in width and depth over the time. Microkarst profile measurements at the limestone statues with profile combs have shown depths of karstification up to 3 cm (Figs. 12, 13). In the worst cases microkarstification results in fragmental disintegration of the limestones (breaking up of the limestone into pieces of variable dimension and irregular shape). Often, microbiological colonization (e.g. lichen) can be observed on the limestones.

3.2. Sandstones

In the following sections monument mapping and ultrasonic measurements are briefly explained from a methodological point of view. Results obtained from the map-



Fig. 11: Weathering of coarsely sparitic veins in the limestone resulting in increase of porosity. SEM-micrograph, image width: ~ 0.12 mm.



Fig. 12: Profile measurements – limestone statues.

ping of weathering forms and from ultrasonic measurements are presented for three exemplar sandstone stelae of the west terrace: Apollo dexiosis stele, Xerxes I stele and Lion Horoscope.

3.2.1 Weathering forms

Weathering forms on stone monuments represent the phenomenological results of weathering processes which are initiated and controlled by interactions between stone and weathering factors. Objective and reproducible registration, documentation, and evaluation of weathering forms requires a precise, standardized classification scheme of weathering forms. Such a classification scheme has been developed, based on the investigation of numerous stone monuments worldwide across different stone types and environments (updated version in Fitzner & Heinrichs 2002, 2004). This classification scheme comprises four levels of differentiation: groups of weathering forms (level I), main weathering forms (level II), individual weathering forms (level III), individual weathering forms with additional differentiation according to intensity (level IV).

Based on a systematic survey of weathering forms on the Nemrud Dag sandstone monuments, the available

standard classification scheme of weathering forms was limited to weathering forms identified on the monuments. A suitable classification of their intensities was integrated. The classification scheme of weathering forms for the Nemrud Dag sandstone monuments is presented in tables 9 and 10. Based on this classification scheme, monument mapping was used to register, document, and evaluate the weathering forms. The mapping method represents a non-destructive, well-established procedure that allows the precise evaluation of entire stone surfaces according to stone type and the type, intensity, and distribution of weathering forms (Fitzner 2004, Fitzner & Heinrichs 2002, 2005). The mapping method can be applied to all kind of natural stones and stone monuments.

Plans of the sandstone monuments selected for mapping were prepared using historical documents to reconstruct their original appearance. The most differentiated level IV of the classification scheme of weathering forms – individual weathering forms, with additional differentiation according to intensity – was used for mapping. Illustrations of weathering forms were made according to groups of weathering forms (group 1 – loss of stone material, group 2 – discoloration/deposits, group 3 – detachment of stone material).

All sandstone monuments of the Nemrud Dag monuments show a limited spectrum of weathering forms. With respect to loss of stone material (group 1 of weathering forms), the main weathering forms are back weathering (W), relief (R) and break out (O). Related individual weathering forms are back weathering due to loss of stone layers dependent on stone structure (xW), rounding/notching (Ro) and break out due to natural cause (nO) (Tab. 9). Regarding discoloration/deposits (group 2 of weathering forms), main weathering forms are discoloration (D), soiling (I), and crust (C). Related individual weathering forms are coloration (Dc), soiling by particles from the atmosphere (pI) and colored crust tracing the morphology of the stone surface (fkC) (Tab. 9). With respect to detachment (group 3 of weathering forms), main weathering forms are granular disintegration (G), crumbly disintegration (P), granular disintegration to crumbly

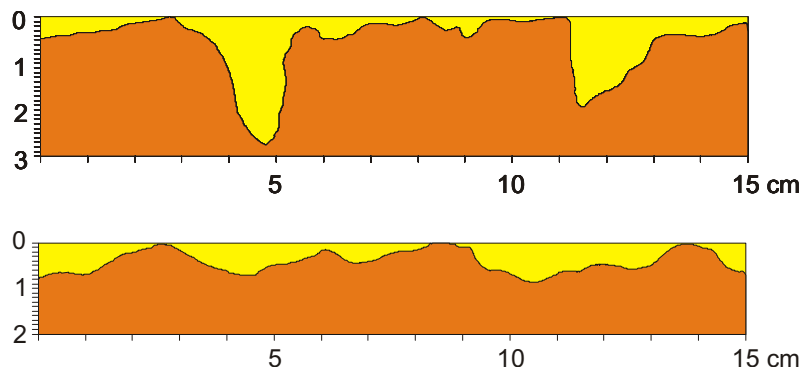


Fig. 13: Microkarst profiles – limestone statues.

Tab. 9: Classification of weathering forms – Nemrud Dag sandstone monuments. Groups 1 and 2 of weathering forms.

| LEVEL I Groups of weathering forms | LEVEL II Main weathering forms | LEVEL III Individual weathering forms | LEVEL IV Classification of intensities |
|---------------------------------------|--|---|--|
| Group 1 – loss of stone material | Back weathering (W) | Back weathering due to loss of stone layers dependent on stone structure (xW) | Parameter: depth of back weathering (cm) Intensity 1: ≤ 0.2 Intensity 2: 0.2–0.5 Intensity 3: 0.5–1 Intensity 4: 1–3 Intensity 5: 3–5 Intensity 6: 5–10 Intensity 7: > 10 |
| | <i>Uniform loss of stone material parallel to the original stone surface.</i> | <i>Uniform loss of stone material parallel to the stone surface due to exfoliation.</i> | |
| | Relief (R) | Rounding / notching (Ro) | Parameter: depth of relief (cm) Intensity 1: ≤ 0.2 Intensity 2: 0.2–0.5 Intensity 3: 0.5–1 Intensity 4: 1–3 Intensity 5: 3–5 Intensity 6: 5–10 Intensity 7: > 10 |
| | <i>Morphological change of the stone surface due to partial or selective weathering.</i> | <i>Relief by rounding of edges or notching / hollowing out. Concave or convex soft forms.</i> | |
| | Break out (O) | Break out due to natural cause (nO) | Parameter: volume of break out (cm ³) Intensity 1: ≤ 1 Intensity 2: 1–5 Intensity 3: 5–50 Intensity 4: 50–250 Intensity 5: 250–1000 Intensity 6: 1000–5000 Intensity 7: > 5000 |
| | <i>Loss of compact stone fragments.</i> | <i>Break out due to earthquakes, natural mechanical impacts etc.</i> | |
| Group 2 – discoloration / deposits | Discoloration (D) | Coloration (Dc) | Parameter: degree – change of color Intensity 1: low Intensity 2: high |
| | <i>Alteration of the original stone color.</i> | <i>Chromatic alteration / coloring due to chemical weathering of minerals, intrusion / accumulation of coloring matter etc.</i> | |
| | Soiling (I) | Soiling by particles from the atmosphere (pI) | Parameter: mass of deposits Intensity 1: low Intensity 2: high |
| | <i>Dirt deposits on the stone surface.</i> | <i>Poorly adhesive, greyish / brownish deposits of dust, mud etc.</i> | |
| | Crust (C) | Colored crust tracing the stone surface (fkC) | Parameter: degree – covering of the stone surface Intensity 1: low Intensity 2: high |
| | <i>Strongly adhesive deposits on the stone surface.</i> | <i>Compact deposit, here very thin brownish crust (clayish-carbonatic), tracing the morphology of the stone surface.</i> | |

Tab. 10: Classification of weathering forms – Nemrud Dag sandstone monuments. Group 3 of weathering forms.

| LEVEL I Groups of weathering forms | LEVEL II Main weathering forms | LEVEL III Individual weathering forms | LEVEL IV Classification of intensities |
|---------------------------------------|--|---|--|
| Group 3 – detachment | Granular disintegration (G) | Granular disintegration into sand (Gs) | Parameter: mass of detaching stone material Intensity 1: low Intensity 2: medium Intensity 3: high |
| | <i>Detachment of individual grains or small grain aggregates.</i> | <i>Detachment of small grains or small grain aggregates in the form of sand.</i> | |
| | Crumbly disintegration (P) | Crumbling (Pu) | Parameter: mass of detaching stone material Intensity 1: low Intensity 2: medium Intensity 3: high |
| | <i>Detachment of larger compact stone pieces (crumbs, splinters) of irregular shape.</i> | <i>Detachment of larger compact stone pieces in the form of crumbs.</i> | |
| | Granular disintegration to crumbly disintegration (G-P) | Granular disintegration into sand to crumbling (Gs-Pu) | Parameter: mass of detaching stone material Intensity 1: low Intensity 2: medium Intensity 3: high |
| | <i>Transitional form between granular disintegration (G) and crumbly disintegration (P).</i> | <i>Transitional form between granular disintegration into sand (Gs) and crumbling (Pu).</i> | |
| | Detachment of stone layers dependent on stone structure (X) | Exfoliation (XI) | Parameter: thickness of the detaching layer resp. stack of layers (cm) Intensity 1: ≤ 0.2 Intensity 2: 0.2–0.5 Intensity 3: 0.5–1 Intensity 4: 1–3 Intensity 5: 3–5 Intensity 6: 5–10 Intensity 7: > 10 |
| | <i>Detachment of sheets or plates following the stone structure.</i> | <i>Detachment of stone layers (sheets, plates) following the bedding structure and the stone surface (bedding structure is oriented parallel to the stone surface).</i> | |

disintegration (G-P) and detachment of stone layers dependent on stone structure (X). Related individual weathering forms are granular disintegration into sand (Gs), crumbling (Pu), granular disintegration into sand to crumbling (Gs-Pu) and exfoliation (XI) (Tab. 10). Exfoliation represents the most significant weathering form characterizing detachment of stone material on the sandstone monuments, taking into consideration that front and back face of all stelae are oriented parallel to bedding of the sandstones (Fig. 14).

Results on weathering forms are presented in the following for the front faces of three representative sandstone monuments: Apollo dexiosis stele, Xerxes I stele and Lion Horoscope of the west terrace (Figs. 15–17). Maps of weathering forms with respect to loss of stone material (group 1 of weathering forms) and detachment (group 3 of weathering forms) are shown for the three sandstone monuments in figures 18–21. The maps show their situation in the year 2002.

Apollo dexiosis stele

With respect to loss of stone material (group 1 of weathering forms), most of the stele is affected by rounding/notching (Fig. 18). Rounding/notching is mainly of intensity 1 (depth of relief: 0.2 cm). The most striking loss of stone material is through back weathering due to exfoliation. It affects the central part of the stele between the reliefs of the King and Apollo. Back weathering occurs with different intensities up to intensity 6 (depth of back weathering: 5–10 cm). Intensity 4 (depth of back weathering: 1–3 cm) is prevailing. Break out due to natural causes affects corners/edges of the stele and smaller parts of the relief, especially parts of the relief of the King. Most striking break out (intensity 5, volume of break out: 250–1000 cm³) concerns the upper right corner of the stele. Loss of stone material did not increase between 1988 and 2002.

Regarding deposits (group 2 of weathering forms), the entire stone surface is covered by a thin brownish crust.



Fig. 14: Weathering form “exfoliation”. Xerxes I stele – west terrace, sandstone.

Intensity 1 and 2 occur with similar portions. Subordinately, coloration is found. Deposits on the stone surface have not changed between 1988 and 2002.



Fig. 15: Apollo dexiosis stele – west terrace, sandstone.



Fig. 16: Xerxes I stele – west terrace, sandstone.

With respect to detachment (group 3 of weathering forms), exfoliation represents the most prevalent and most significant weathering form (Fig. 19). Exfoliation occurs with different intensities up to intensity 6 (thickness of the detaching layer/stack of layers: 5–10 cm). Intensity 4 (thickness of the detaching layer/stack of layers: 1–3 cm) is prevailing. Exfoliation mainly affects the central part of the stele and the right part of the relief of the King. Different phases of exfoliation have taken place over the time. Comparing the maps from 1988 and 2002, exfoliation of intensity 6 is seen to have extended in the direction of the left relief (the King). Granular disintegration, crumbling and their transitional form represent additional weathering forms characterizing the detachment of stone material. They are mainly of intensity 1 (mass of detaching stone material: low).

Xerxes I stele

In terms of the loss of stone material, most of the stele is affected by rounding/notching (Fig. 18). Intensity 1 of



Fig. 17: Lion Horoscope – west terrace, sandstone.

this weathering form is most prevalent (depth of relief: 0.2 cm). The most significant weathering form characteristic of the loss of stone material is back weathering due to exfoliation. It affects especially the right part of the Xerxes I relief with intensities 4 and 5 (depth of back weathering: 1–3 cm, resp. 3–5 cm). From 1988 to 2002 back weathering due to exfoliation has slightly increased. Break out due to natural causes affects corners/edges of the stele and parts of the relief. The most striking break out (intensity 6, volume of break out: 1000–5000 cm³) is seen on the left edge of the stele.

In terms of deposits, the entire stone surface is covered by a thin brownish crust. Intensity 2 is prevailing. Subordinately, soiling by particles from the atmosphere is found. Deposits on the stone surface have not changed between 1988 and 2002.

With respect to detachment, exfoliation is the most prevalent and most significant weathering form (Fig. 19). Exfoliation occurs with different intensities up to intensity 6 (thickness of the detaching layer/stack of layers: 5–10 cm), although intensity 4 (thickness of the detaching layer/stack of layers: 1–3 cm) predominates. Exfoliation mainly affects the Xerxes I relief. Comparing the maps from 1988 and 2002, it is found that exfoliation of intensity 6 has extended to the head of the Xerxes I relief. Granular disintegration, crumbling, and their transitional form occur as additional weathering forms characterizing detachment of stone material. They are only of intensity 1 (mass of detaching stone material: low) and they mainly concern edges/corners of the stele.

Lion Horoscope

With respect to loss of stone material, most of the stele is affected by rounding/notching (Fig. 20). Rounding/notching up to intensity 4 (depth of relief: 1–3 cm) can be stated, although intensity 1 of this weathering form is prevailing (depth of relief: 0.2 cm). Most significant weathering form characterizing loss of stone material is back weathering

due to exfoliation. It affects large parts of the lion relief. Back weathering occurs with different intensities. Intensities 5–7 (depth of back weathering: 3–5 cm, 5–10 cm, > 10 cm) are prevailing. From 1988 to 2002 back weathering due to exfoliation has significantly increased, especially concerning the left part of the lion relief. Break out due to natural causes concerns corners / edges of the stele and parts of the relief (especially claws of the lion, intensities 5 and 7 – volume of break out: 250–1000 cm³, resp. > 5000 cm³). One larger part of the lion relief has broken off in the period between 1988 and 2002.

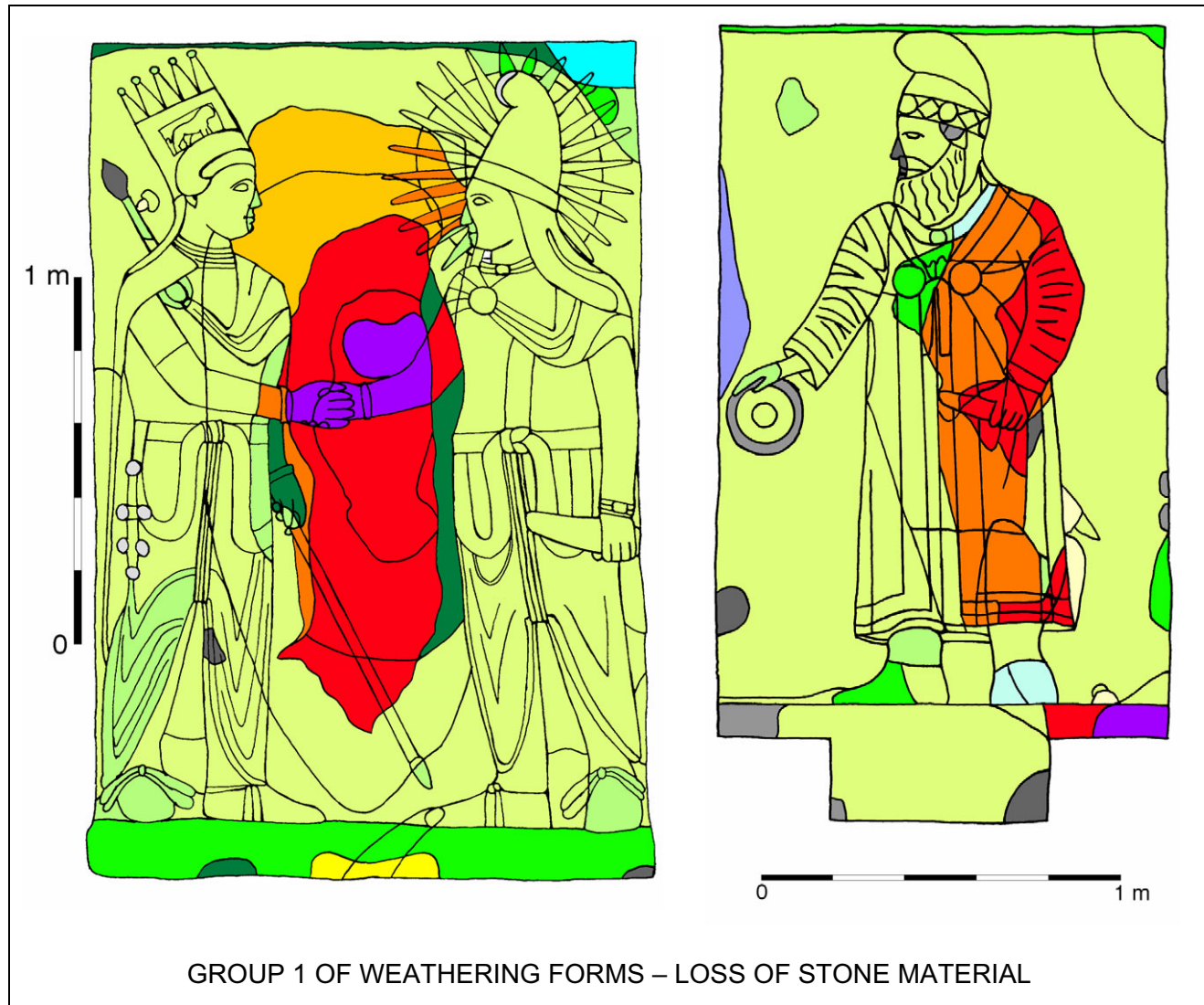
In terms of deposits, the entire stone surface is covered by a thin brownish crust. Intensity 2 occur is prevailing. “Fresh” surfaces due to back weathering or break out short time ago do not show new crust formation until now.

Regarding detachment of stone material, exfoliation is the most prevalent and most significant weathering form (Fig. 21). Exfoliation occurs with different intensities up to intensity 7 (thickness of the detaching layer/stack of layers: > 10 cm). Intensity 5 (thickness of the detaching layer/stack of layers: 3–5 cm) predominates. Exfoliation mainly affects the relief of the lion. Comparing the maps from 1988 and 2002, it is found that exfoliation has slightly extended over the surface of the relief. However, owing to back weathering due to exfoliation over the last years, intensity of exfoliation is partly reduced (secondary generations of exfoliation with lower thickness of detaching layers/stack of layers). Granular disintegration, crumbling and their transitional form occur as additional weathering forms characterizing detachment of stone material. They are mainly of intensity 1 (mass of detaching stone material: low).

3.2.2. Ultrasonic velocities

Ultrasonic measurements represent a suitable non-destructive method for information on the state of weathering. Ultrasonic measurements were carried out at the Apollo dexiosis stele and the Lion Horoscope of the west terrace. Grids of measuring points were arranged on the front side of the stelae (Figs. 22, 23) and then were transferred to their rear side. The distances between corresponding measuring points were determined. Ultrasonic measurements were made according to transmission mode. The ultrasonic velocities were calculated from transit time and measured distance. They were illustrated in maps, based on isoline calculations.

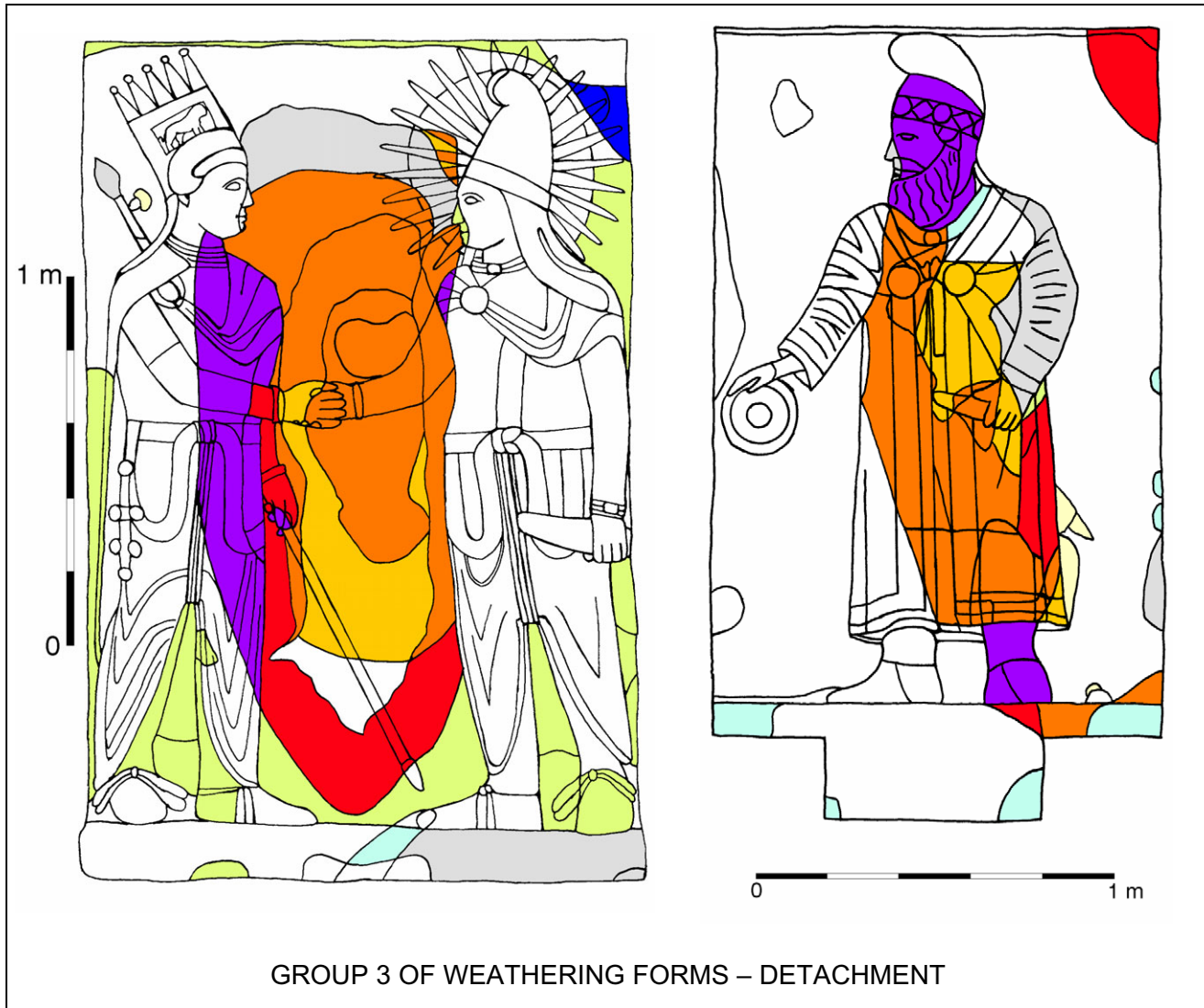
The maps of ultrasonic velocities for the Apollo dexiosis stele and the Lion Horoscope are presented in figures 24 and 25. Decreasing ultrasonic velocities (indicated by colour change from blue via green and yellow to red) correspond to increasing physical disintegration of the sandstone (granular or crumbly disintegration, exfoliation). Very low ultrasonic velocities mainly correspond with exfoliation of the sandstone. Comparing the maps of ul-



| | | | | | | | |
|---|---|--------------------------|------------------------|-------------------------|---------------------------|--------------------------|-----------------------|
| Back weathering due to loss of stone layers dependent on stone structure (xW) | <i>Depth of back weathering (cm)</i> | | | | | | |
| | Intensity 1 ≤ 0.2 | Intensity 2 0.2 - 0.5 | Intensity 3 0.5 - 1 | Intensity 4 1 - 3 | Intensity 5 3 - 5 | Intensity 6 5 - 10 | Intensity 7 > 10 |
| Rounding / notching (Ro) | <i>Depth of relief (cm)</i> | | | | | | |
| | Intensity 1 ≤ 0.2 | Intensity 2 0.2 - 0.5 | Intensity 3 0.5 - 1 | Intensity 4 1 - 3 | Intensity 5 3 - 5 | Intensity 6 5 - 10 | Intensity 7 > 10 |
| Break out due to natural cause (nO) | <i>Volume of break out (cm³)</i> | | | | | | |
| | Intensity 1 ≤ 1 | Intensity 2 1 - 5 | Intensity 3 5 - 50 | Intensity 4 50 - 250 | Intensity 5 250 - 1000 | Intensity 6 1000-5000 | Intensity 7 > 5000 |

Fig. 18: Map of the weathering forms of group 1 – loss of stone material (2002). Apollo dexiosis stele (left) and Xerxes I stele (right) – west terrace, sandstone.

Fig. 19: Map of the weathering forms of group 3 – detachment (2002). Apollo dexiosis stele (left) and Xerxes I stele (right) – west terrace, sandstone.



GROUP 3 OF WEATHERING FORMS – DETACHMENT

| | | | | | | | |
|--|---|--|--|--|--|--|--|
| Granular disintegration into sand (Gs) | <p style="text-align: center;"><i>Mass of detaching stone material</i></p> <p style="text-align: center;">Intensity 1 Intensity 2 Intensity 3</p> <p style="text-align: center;">low medium high</p> <div style="display: flex; justify-content: space-around; width: 100%;"> <div style="width: 33%; height: 10px; background-color: #90EE90;"></div> <div style="width: 33%; height: 10px; background-color: #FFFF00;"></div> <div style="width: 33%; height: 10px; background-color: #FF0000;"></div> </div> | | | | | | |
| Crumbling (Pu) | <p style="text-align: center;"><i>Mass of detaching stone material</i></p> <p style="text-align: center;">Intensity 1 Intensity 2 Intensity 3</p> <p style="text-align: center;">low medium high</p> <div style="display: flex; justify-content: space-around; width: 100%;"> <div style="width: 33%; height: 10px; background-color: #00FFFF;"></div> <div style="width: 33%; height: 10px; background-color: #FF0000;"></div> <div style="width: 33%; height: 10px; background-color: #0000FF;"></div> </div> | | | | | | |
| Granular disintegration into sand to crumbling (Gs – Pu) | <p style="text-align: center;"><i>Mass of detaching stone material</i></p> <p style="text-align: center;">Intensity 1 Intensity 2 Intensity 3</p> <p style="text-align: center;">low medium high</p> <div style="display: flex; justify-content: space-around; width: 100%;"> <div style="width: 33%; height: 10px; background-color: #A9A9A9;"></div> <div style="width: 33%; height: 10px; background-color: #FF0000;"></div> <div style="width: 33%; height: 10px; background-color: #0000FF;"></div> </div> | | | | | | |
| Exfoliation (XI) | <p style="text-align: center;"><i>Thickness of the detaching layer resp. stack of layers (cm)</i></p> <p style="text-align: center;">Intensity 1 Intensity 2 Intensity 3 Intensity 4 Intensity 5 Intensity 6 Intensity 7</p> <p style="text-align: center;">≤ 0.2 0.2 - 0.5 0.5 - 1 1 - 3 3 - 5 5 - 10 > 10</p> <div style="display: flex; justify-content: space-around; width: 100%;"> <div style="width: 14%; height: 10px; background-color: #FFFF00;"></div> <div style="width: 14%; height: 10px; background-color: #FFA500;"></div> <div style="width: 14%; height: 10px; background-color: #FF4500;"></div> <div style="width: 14%; height: 10px; background-color: #FF0000;"></div> <div style="width: 14%; height: 10px; background-color: #FF00FF;"></div> </div> | | | | | | |

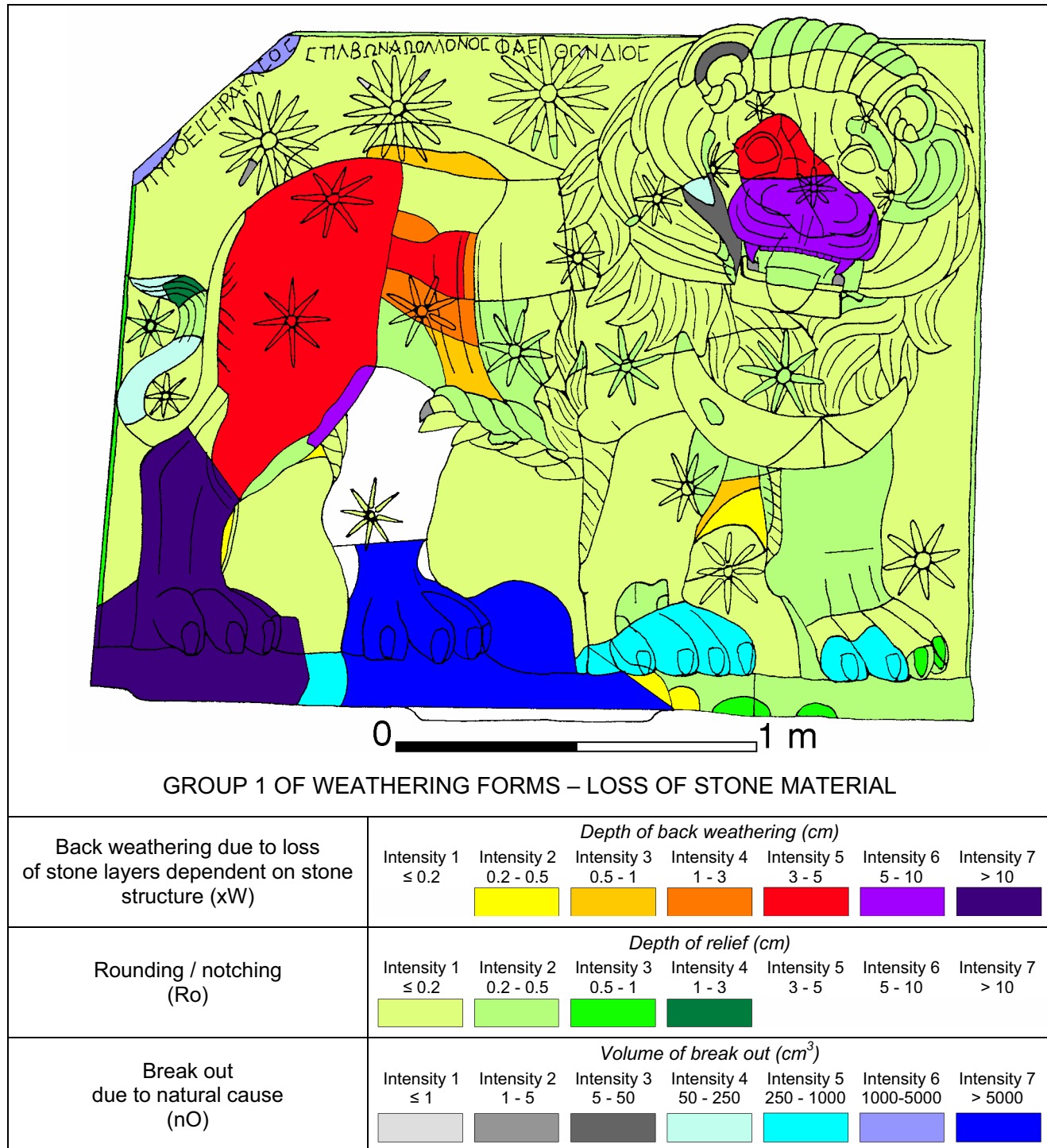


Fig. 20: Map of the weathering forms of group 1 – loss of stone material (2002). Lion Horoscope – west terrace, sandstone.

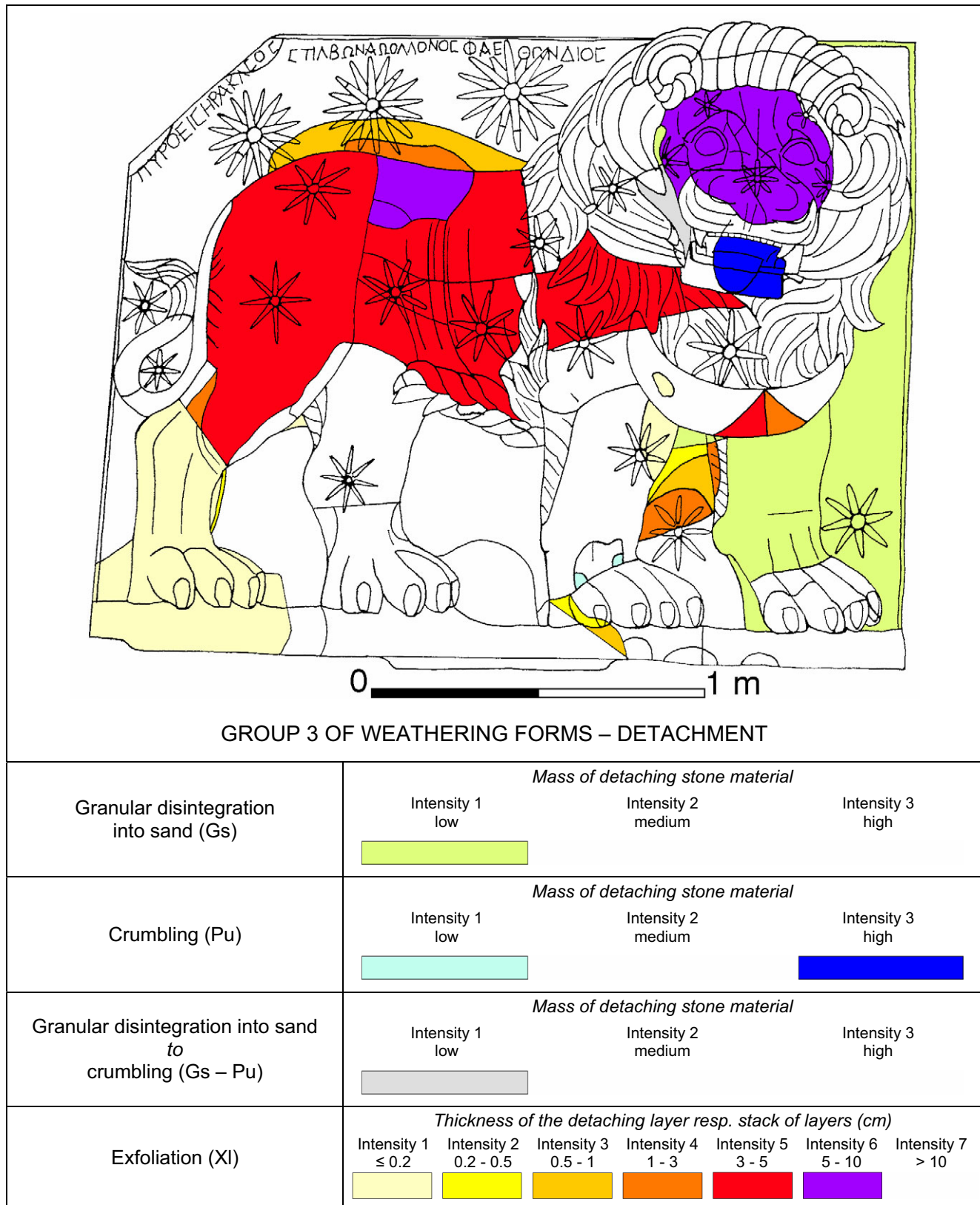


Fig. 21: Map of the weathering forms of group 3 – detachment (2002). Lion Horoscope – west terrace, sandstone.



Fig. 22: Grid of measuring points for ultrasonic measurements. Apollo dexiosis stele – west terrace, sandstone.

trasonic velocities with maps of weathering forms characteristic of the detachment of stone material, the presence of considerable non-visible disintegration and detachment of stone material can be additionally identified, especially in the case of the Lion Horoscope.

3.2.3. Rating of weathering damage

While weathering forms are used for the precise description of weathering characteristics according to phenomenological-geometrical criteria, damage categories and damage indices have been introduced for the rating of weathering damage (Fitzner & Heinrichs 2002, Fitzner et al. 2002). Damage categories are used for the individual rating of the weathering forms with respect to degree of damage, the damage indices are applied for the overall quantification and rating of weathering damage on stone monuments. Damage categories and damage indices can be considered as suitable indicators of need and urgency of preservation measures. Six damage categories were de-

finied: 0 – no damage, 1 – very slight damage, 2 – slight damage, 3 – moderate damage, 4 – severe damage, 5 – very severe damage. A correlation scheme “weathering forms – damage categories” was developed especially for the Nemrud Dag sandstone monuments, in which all weathering forms – type and intensity – are related to damage categories (Tab. 11). The high historical and artistical importance of the monuments was taken into account. Based on this correlation scheme, damage categories were determined separately for loss of stone material, discoloration/deposits, and detachment. Final damage categories were derived by jointly considering all weathering forms of the three groups (Fig. 26). The damage categories were illustrated in maps and evaluated quantitatively. Damage indices – linear damage index DI_{lin} and progressive damage index DI_{prog} – were defined as numerical parameters for the conclusive quantification and rating of weathering damage. Their calculation is based on the quantitative evaluation of the damage categories (Fig. 27). The linear damage index corresponds to average damage category, whereas the progressive damage index emphasizes the portion of higher damage categories and, thus, emphasizes the need and urgency of preservation measures. Linear damage index as well as progressive damage index can range between 0 and 5 as per definition.

In figure 28 the maps of final damage categories with quantitative evaluation are presented for the front faces of Apollo dexiosis stele, Xerxes I stele, and Lion Horoscope. They relate to the year 2002. The surfaces of all stelae are entirely affected by damage. Very slight damage is prevailing (Apollo dexiosis stele: 53 %, Xerxes I stele: 67 %, Lion Horoscope: 48 %). However, the very high portion of severe to very severe damage is most alarming (Apollo dexiosis stele: 36 %, Xerxes I stele: 28 %, Lion Horoscope: 39 %). Comparing the three stelae, the overall extent of damage increases from Xerxes I stele via Apollo dexiosis stele to Lion Horoscope (Xerxes



Fig. 23: Ultrasonic measurements. Lion Horoscope – west terrace, sandstone.

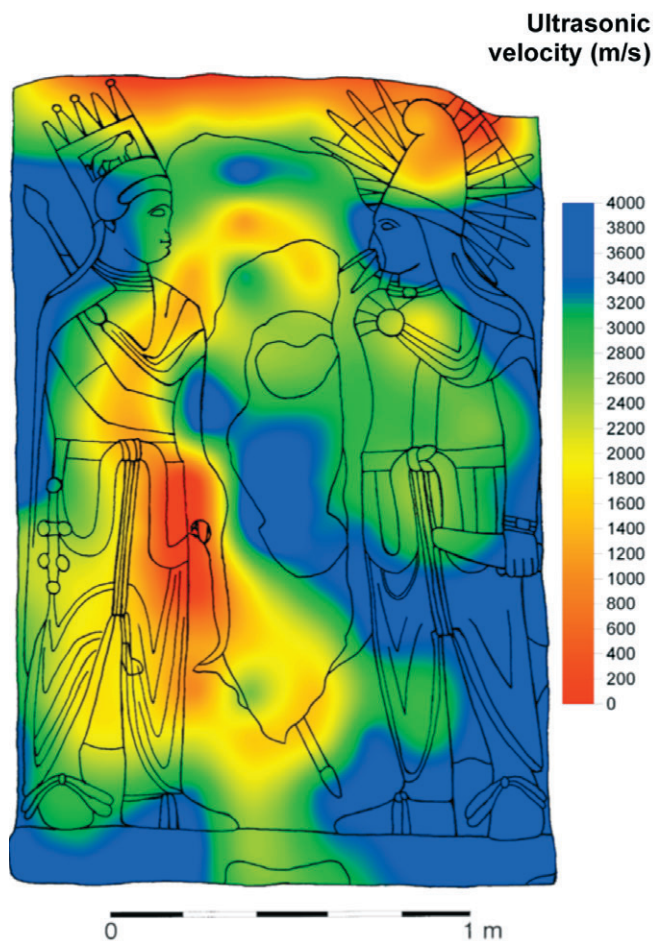


Fig. 24: Map of ultrasonic velocities (2002). Apollo dexiosis stele – west terrace, sandstone.

I stele: $DI_{lin} = 2.09$, $DI_{prog} = 2.66$, Apollo dexiosis stele: $DI_{lin} = 2.57$, $DI_{prog} = 3.14$, Lion Horoscope: $DI_{lin} = 2.70$, $DI_{prog} = 3.28$). When comparing Xerxes I stele and Apollo dexiosis stele, it should be considered that very severe damage on the Xerxes I stele affects parts of the relief to higher extent than on the Apollo dexiosis stele.

The results gathered from the ultrasonic measurements attest alarming extent of weathering damage, too. They reveal higher extent of damage for the Lion Horoscope (reduction of ultrasonic velocities: ~ 55 % on average) in comparison with the Apollo dexiosis stele (reduction of ultrasonic velocities: ~ 30 % on average). This confirms the ranking derived from evaluation of damage indices. The results in all indicate the need of monument preservation measures.

3.2.4. Weathering progression

The characterization, quantification, and prognosis of weathering progression is an important concern of scientific damage diagnosis. Photo documentation of the Nemrud

Dag sandstone monuments made in 1988 and 2002 have visualized partly significant increase of weathering damage within that short period of fourteen years considering more than 2000 years of exposure. Weathering damage on the Apollo dexiosis stele, Xerxes I stele, and Lion Horoscope has increased between 1988 and 2002, too, as shown by increase of damage indices (Figs. 29 and 30). Xerxes I stele and Lion Horoscope show higher increase of damage than the Apollo dexiosis stele. In the cases of the Apollo dexiosis stele and the Xerxes I stele increase of damage finds expression in extended detachment of stone material, whereas in case of the Lion Horoscope it is due to increased loss of stone material. Considering that recent detachment of stone material sometime will result in loss of stone material, the three stelae are in considerable danger regarding future loss of stone material. This can be deduced from the damage indices relating to detachment. Here, highest risk can be stated for the Apollo dexiosis stele, followed by Lion Horoscope and Xerxes I stele.

For further assessment of weathering progression, a photograph of the Lion Horoscope from 1953 (in Sanders 1996), a photograph of the Xerxes I stele from 1956 (Sanders 1996) and a photograph of a gypsum replica of the Xerxes I stele made in 1883 (Dörner 1987) were considered as references. The photos were evaluated with respect to loss of stone material (weathering forms – damage categories – damage indices). This has allowed comparison of the loss of stone material over a period of 49 years for the Lion Horoscope (1953–2002) and 119 years for the Xerxes I stele (1883–2002). The results are presented in figures 31 and 32. The graphs show the alarming increase of damage over the last century. The fact that there was no further loss of stone material on the Xerxes I stele between 1988 and 2002 should not be misinterpreted in this regard. Detachment of stone material has extended in that period and this will result in further loss of stone material, probably in near future.

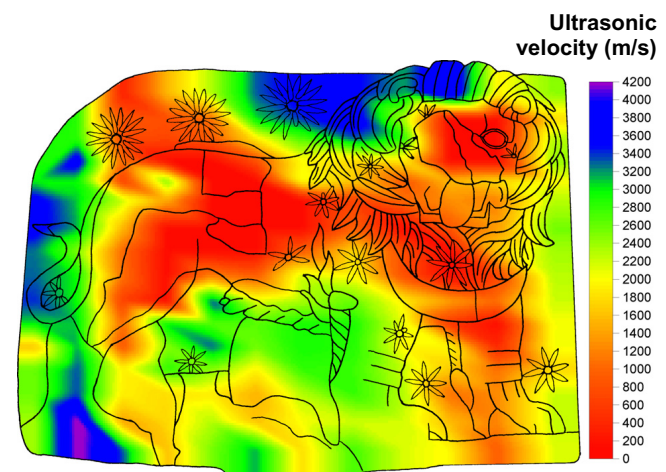


Fig. 25: Map of ultrasonic velocities (2002). Lion Horoscope – west terrace, sandstone.

Tab. 11: Correlation scheme “weathering forms – damage categories” for the Nemrud Dag sandstone monuments.

| | | | |
|----------|--|----------|--|
| 0 | Damage category 0 – no damage | 3 | Damage category 3 – moderate damage |
| 1 | Damage category 1 – very slight damage | 4 | Damage category 4 – severe damage |
| 2 | Damage category 2 – slight damage | 5 | Damage category 5 – very severe damage |

GROUP 1 OF WEATHERING FORMS – LOSS OF STONE MATERIAL

| Back weathering due to loss of stone layers dependent on stone structure (xW) | <i>Depth of back weathering (cm)</i> | | | | | | |
|---|---|------------------------|----------------------|-----------------------|-------------------------|--------------------------|-----------------------|
| | Intensity 1 ≤ 0.2 | Intensity 2 0.2–0.5 | Intensity 3 0.5–1 | Intensity 4 1–3 | Intensity 5 3–5 | Intensity 6 5–10 | Intensity 7 > 10 |
| | 1 | 2 | 3 | 4 | 5 | 5 | 5 |
| Rounding / notching (Ro) | <i>Depth of relief (cm)</i> | | | | | | |
| | Intensity 1 ≤ 0.2 | Intensity 2 0.2–0.5 | Intensity 3 0.5–1 | Intensity 4 1–3 | Intensity 5 3–5 | Intensity 6 5–10 | Intensity 7 > 10 |
| | 1 | 2 | 3 | 4 | 5 | 5 | 5 |
| Break out due to natural cause (nO) | <i>Volume of break out (cm³)</i> | | | | | | |
| | Intensity 1 ≤ 1 | Intensity 2 1–5 | Intensity 3 5–50 | Intensity 4 50–250 | Intensity 5 250–1000 | Intensity 6 1000–5000 | Intensity 7 > 5000 |
| | 1 | 2 | 3 | 4 | 5 | 5 | 5 |

GROUP 2 OF WEATHERING FORMS – DISCOLORATION / DEPOSITS

| Coloration (Dc) | <i>Degree – change of color</i> | |
|---|---|---------------------|
| | Intensity 1 low | Intensity 2 high |
| | 1 | 1 |
| Soiling by particles from the atmosphere (pl) | <i>Mass of deposits</i> | |
| | Intensity 1 low | Intensity 2 high |
| | 1 | 1 |
| Colored crust tracing the surface (fkC) | <i>Degree - covering of the stone surface</i> | |
| | Intensity 1 low | Intensity 2 high |
| | 1 | 1 |

Tab. 11: Cont.

| GROUP 3 OF WEATHERING FORMS – DETACHMENT | | | | | | | |
|---|--|------------------------|----------------------|---------------------|--------------------|---------------------|---------------------|
| Granular disintegration into sand (Gs) | <i>Mass of detaching stone material</i> | | | | | | |
| | Intensity 1 low | Intensity 2 medium | | Intensity 3 high | | | |
| | 1 | 2 | | 3 | | | |
| Crumbling (Pu) | <i>Mass of detaching stone material</i> | | | | | | |
| | Intensity 1 low | Intensity 2 medium | | Intensity 3 high | | | |
| | 2 | 3 | | 4 | | | |
| Granular disintegration into sand to crumbling (Gs – Pu) | <i>Mass of detaching stone material</i> | | | | | | |
| | Intensity 1 low | Intensity 2 medium | | Intensity 3 high | | | |
| | 2 | 3 | | 4 | | | |
| Exfoliation (XI) | <i>Thickness of the detaching layer resp. stack of layers (cm)</i> | | | | | | |
| | Intensity 1 ≤ 0.2 | Intensity 2 0.2–0.5 | Intensity 3 0.5–1 | Intensity 4 1–3 | Intensity 5 3–5 | Intensity 6 5–10 | Intensity 7 > 10 |
| | 1 | 2 | 3 | 4 | 5 | 5 | 5 |

4. Summary and conclusions

Studies were carried out in 1988 and 2002 on the stone monuments of the Nemrud Dag sanctuary/East Turkey built in the first century B.C. by King Antiochos I of Commagene. The studies aimed at the diagnosis of stone materials and weathering damage on the stone monuments.

Preliminary studies addressed the colossal limestone statues. The whitish, massive limestones can be characterized as pure limestones. Composition varies significantly regarding proportion of sparite, micrite, and bioclasts. Networks of coarsely sparitic veins are characteristic for the limestones. The total porosity of the limestones is very low and consists predominantly of micropores. The main weathering phenomena are the loss of compact stone fragments, cracks and especially microkarst. Microkarst formation on the limestones often originates from disintegration of the coarsely sparitic veins in the limestones resulting in increase of porosity. In the worst cases microkarst formation results in fragmental disintegration of the limestones. The investigation of the limestone monuments needs to be extended to provide more detailed information on weathering behaviour and extent of damage.

Very detailed studies were carried out on the sandstone monuments (stelae with reliefs, sculptures) including laboratory analysis and in-situ investigation (monu-

ment mapping, ultrasonic measurements). Results for petrographical properties, state of weathering, extent of weathering damage, and weathering progression were obtained from these diagnostical studies.

The sandstones – greenish to greyish in colour – represent rather hard, very matrix-rich, fine- to medium-grained sandstones with parallel bedding. Partly, their fabric is considerably anisotropic. The sandstones are composed of quartz, feldspar, rock fragments, chlorite, mica, heavy minerals, and matrix (carbonatic matrix > non-carbonatic matrix). The proportion of components and grain size distribution vary significantly. The sandstones are characterized by low total porosity. Smaller capillary pores are prevailing. With increasing grain/matrix ratio and mean grain size, as a trend total porosity, proportion of capillary pores, capillary pores/micropores ratio, median radius of pore entries, water uptake, and water penetration capacity of the sandstones increase, too. Increasing proportion of micropores correlates with increasing pore surface, adsorption of air humidity, and retain of residual water in the course of evaporation. Although the sandstones show a considerable range in their petrographical properties, a subdivision into different lithotypes is not suitable as the petrographical range is characterized by smooth transitions.

The sandstone monuments are affected by loss of stone material, deposits on the stone surface and detach-

| | | | | | | | | | |
|--|---|---|---|---|---|---|---|--|--|
| | | Damage categories considering all groups of weathering forms | | | | | | | |
| Damage categories for the weathering forms of group 1 – loss of stone material | 0 | 0 | 1 | 2 | 3 | 4 | 5 | Damage categories for the weathering forms of group 2 – discoloration / deposits | |
| | 1 | 1 | 1 | 2 | 3 | 4 | 5 | | |
| | 2 | 1 | 1 | 2 | 3 | 4 | 5 | | |
| | 3 | 2 | 2 | 2 | 3 | 4 | 5 | | |
| | 4 | 2 | 2 | 2 | 3 | 4 | 5 | | |
| | 5 | 3 | 3 | 3 | 3 | 4 | 5 | | |
| | | Damage categories for the weathering forms of group 3 – detachment | | | | | | | |
| | | 0 | 1 | 2 | 3 | 4 | 5 | | |

Fig. 26: Scheme for the determination of final damage categories considering the three groups of weathering forms, developed for the Nemrud Dag sandstone monuments.

ment of stone material. Characteristic weathering forms are back weathering due to exfoliation, relief (rounding/notching), break out due to natural causes, discoloration, soiling, crust (carbonatic-clayish), granular to crumbly disintegration, and exfoliation. Exfoliation and subsequent back weathering due to exfoliation represent the most significant weathering forms harming the sandstone monuments. Often they occur with high intensities. Larger parts of many reliefs are lost already or recently underlie the process of detachment.

The spectrum of weathering forms indicates that primarily physical weathering causes the damage on the sandstone monuments. Thermal and hygric expansion and frost weathering are considered as the major weathering processes. Both mechanisms, wetting/drying and freezing/thawing exert stress on the outer layers of the sandstones resulting in loosening of intergranular bonds. The internal stress often results in physical separation of the sandstones into individual stone layers along plane interfaces (exfoliation). This effect is intensified for the reasons of anisotropy of the sandstones and the stone structure (bedding) being oriented parallel to the stone surface of the monuments.

Damage categories and damage indices have turned out as very suitable tools for the rating of weathering damage. High proportions of severe or even very severe damage on many Nemrud Dag sandstone monuments are alarming. The historical and artistic expressiveness of many sandstone monuments is endangered, if not already reduced significantly.

Information on weathering progression – derived from results of the 1988 and 2002 field campaigns and from additional consideration of archive documents – has revealed a remarkable increase of weathering damage over the last century. This leads to alarming risk prognoses for most of the sandstone monuments in the case of non-intervention.

The results of the diagnostical studies in all indicate the need of interventions for monument preservation. They enhance the planning and implementation of appropriate monument preservation measures. This concerns immediate safeguarding measures, measures for the reduction of causes of damage, measures for remedy of damage and preventive measures. The following types of preservation measures should be taken into consideration: re-erection/re-arrangement, protection of the monuments against further loss of stone material (e.g. fixation of detaching stone

$$\begin{aligned}
 & \text{LINEAR DAMAGE INDEX } \mathbf{DI}_{\text{lin}} \\
 &= \frac{(A \cdot 0) + (B \cdot 1) + (C \cdot 2) + (D \cdot 3) + (E \cdot 4) + (F \cdot 5)}{100} \\
 &= \frac{B + (C \cdot 2) + (D \cdot 3) + (E \cdot 4) + (F \cdot 5)}{100}
 \end{aligned}$$

$$\begin{aligned}
 & \text{PROGRESSIVE DAMAGE INDEX } \mathbf{DI}_{\text{prog}} \\
 &= \sqrt{\frac{(A \cdot 0^2) + (B \cdot 1^2) + (C \cdot 2^2) + (D \cdot 3^2) + (E \cdot 4^2) + (F \cdot 5^2)}{100}} \\
 &= \sqrt{\frac{B + (C \cdot 4) + (D \cdot 9) + (E \cdot 16) + (F \cdot 25)}{100}}
 \end{aligned}$$

- A = Area (%) – damage category 0
- B = Area (%) – damage category 1
- C = Area (%) – damage category 2
- D = Area (%) – damage category 3
- E = Area (%) – damage category 4
- F = Area (%) – damage category 5

$$\begin{aligned}
 \sum_A^F &= 100 \\
 0 &\leq \mathbf{DI}_{\text{lin}} \leq 5 \\
 0 &\leq \mathbf{DI}_{\text{prog}} \leq 5 \\
 \mathbf{DI}_{\text{lin}} &\leq \mathbf{DI}_{\text{prog}}
 \end{aligned}$$

Fig. 27: Linear and progressive damage index.

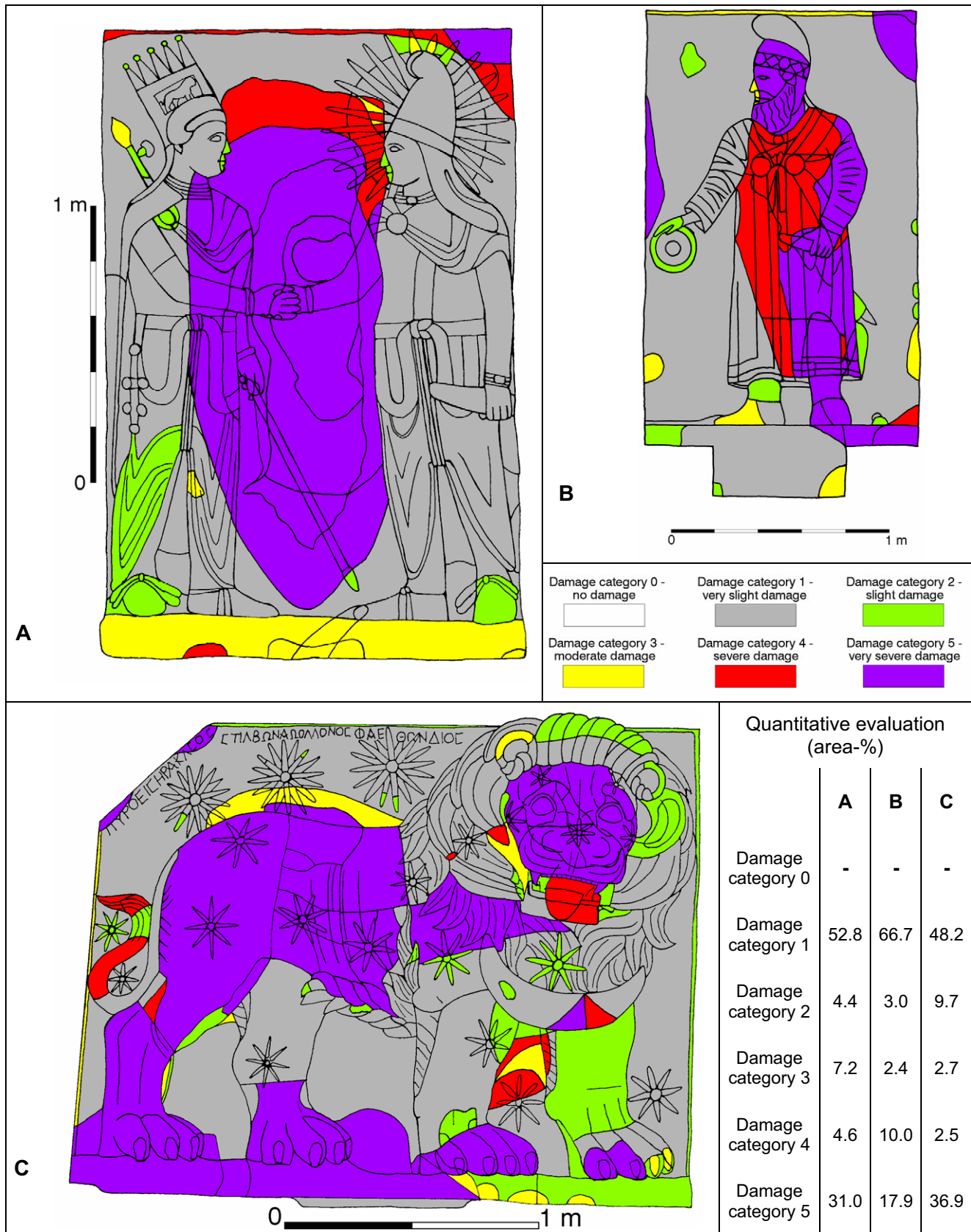


Fig. 28: Maps of final damage categories with quantitative evaluation (2002). A = Apollo dexiosis stele, B = Xerxes I stele, C = Lion Horoscope. West terrace, sandstone.

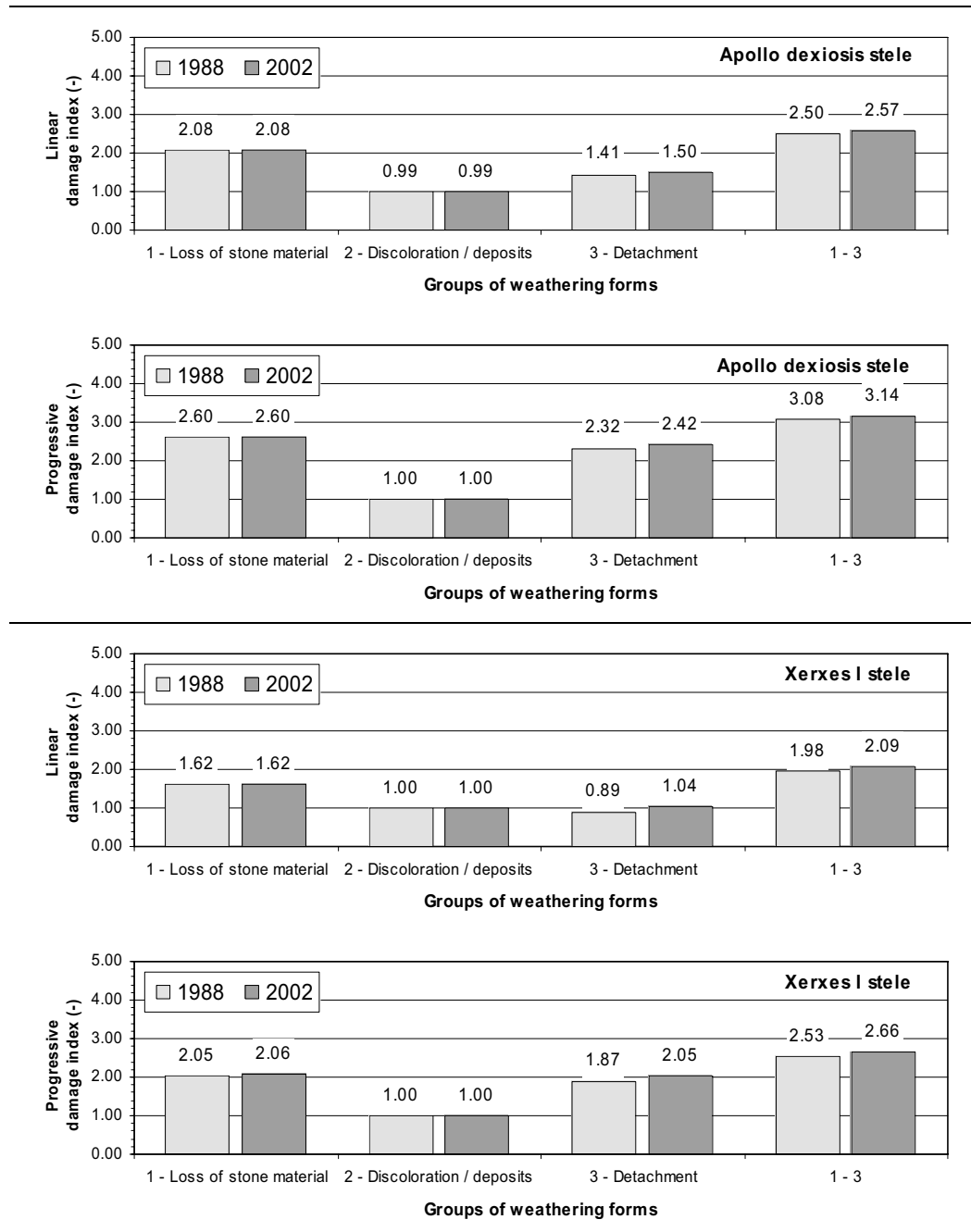


Fig. 29: Comparison of linear and progressive damage indices in 1988 and 2002. Apollo dexiosis stele and Xerxes I stele – west terrace, sandstone.

material), structural stabilization/reinforcement, stone repair, surface protection, sheltering, relocation/replacement by replica. Careful test applications are strongly recommended in order to check applicability and success of the selected monument preservation measures.

5. Acknowledgements

The authors would like to express their gratitude to the World Monuments Fund (WMF) for the support of the field campaign in the year 2002.

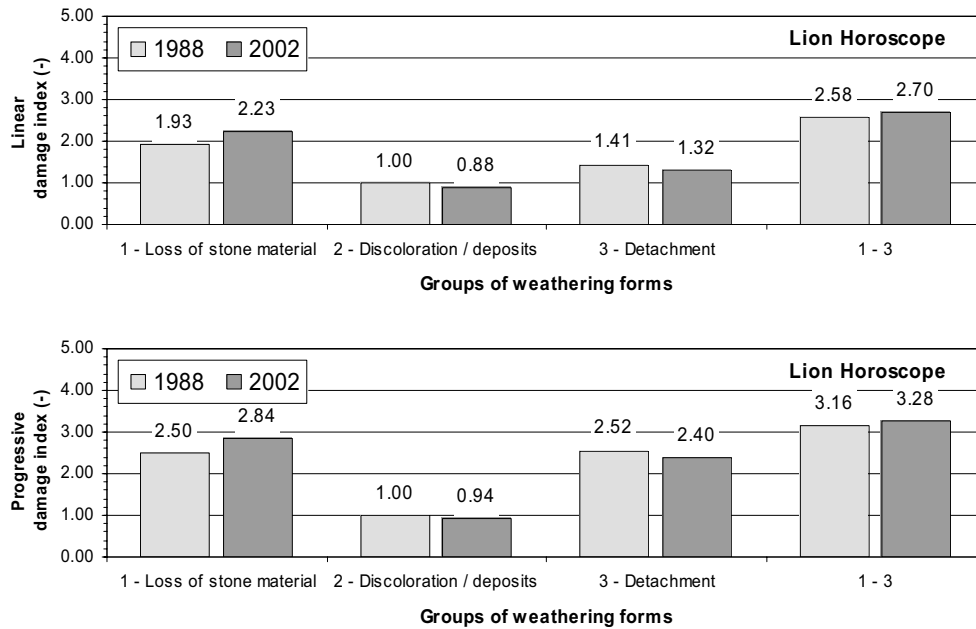


Fig. 30: Comparison of linear and progressive damage indices in 1988 and 2002. Lion Horoscope – west terrace, sandstone.

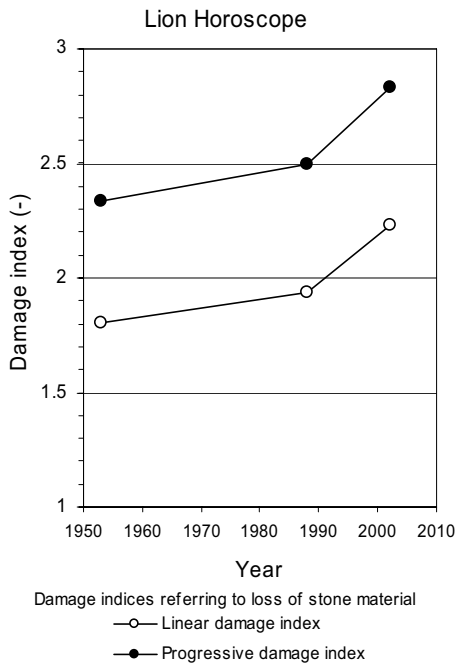


Fig. 31: Weathering progression. Lion Horoscope – west terrace, sandstone.

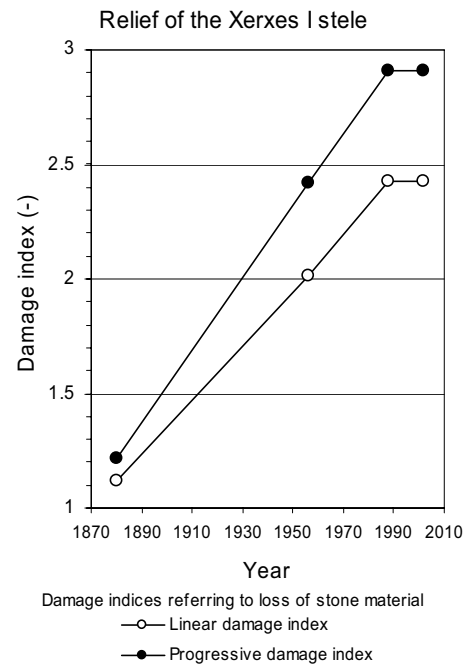


Fig. 32: Weathering progression. Relief of the Xerxes I stele – west terrace, sandstone.

6. References

- Dörner, K.F. (1987): Der Thron der Götter auf dem Nemrud Dag – Kommagene, das große archäologische Abenteuer der östlichen Türkei, 2. Aufl.: 264 p., Bergisch Gladbach (Lübbe).
- Fitzner, B. (2004): Assessment of weathering damage on stone monuments. – In: Akasheh, T.S. (ed.): First International Conference on Science and Technology in Archaeology and Conservation, Actas: 171–207, Granada (Fundación El Legado Andalusi).
- Fitzner, B. & Düppenbecker, V. (1991): Gesteinseigenschaften und Verwitterungszustand der Monumente auf dem Nemrud Dag. – In: Begleitheft zur Sonderausstellung „Nemrud Dag – Neue Methoden der Archäologie“ des Westfälischen Museums für Archäologie und des Westfälischen Museumsamtes Münster: 39–45 und 66–72, Bönen Westfalen.
- Fitzner, B. & Heinrichs, K. (2002): Damage diagnosis on stone monuments – weathering forms, damage categories and damage indices. – In: Prikryl, R. & Viles, H.A. (eds.): Understanding and managing stone decay. – Proceeding Internat. Conf. “Stone weathering and atmospheric pollution network (SWAPNET)”: 11–56, Charles Univ. Prague (Karolinum Press).
- Fitzner, B. & Heinrichs, K. (2004): Photo atlas of weathering forms on stone monuments: www.stone.rwth-aachen.de.
- Fitzner, B. & Heinrichs, K. (2005): Kartierung und Bewertung von Verwitterungsschäden an Natursteinbauwerken. – Z. dt. Ges. Geowiss., 156 (1): 7–24, Stuttgart (Schweizerbart).
- Fitzner, B., Heinrichs, K. & La Bouchardiere, D. (2002): Damage index for stone monuments. – In: Galan, E. & Zezza, F. (eds.): Protection and conservation of the cultural heritage of the Mediterranean cities: Proceedings of the 5th International symposium on the conservation of monuments in the Mediterranean basin: 315–326, Lisse (Swets & Zeitlinger).
- Fitzner, B., Heinrichs, K. & La Bouchardiere, D. (2003): Diagnosis of weathering damage. – In: Moormann, E.M. & Versluys, M.J.: The Nemrud Dag Project: second interim report: BABesch 78 (2003): 159–166.
- Humann, K. & Puchstein, O. (1890): Reisen in Kleinasien und Nordsyrien; 2 Bde., Berlin (Reimer).
- Pettijohn, F.J., Potter, P.E. & Siever, R. (1987): Sand and sandstone, 2nd edition, New York (Springer).
- Sanders, D.H. (ed.) (1996): Nemrud Dagi. The hierothesion of Antiochios I of Commagene. Results of the American excavations directed by Theresa B. Goell, Winona Lake, IN (Eisenbrauns).
- The Geological Society of America (1991): Rock-color chart with genuine Munsell color chips.
- Tucker, M. (1988): Techniques in sedimentology: 394 p., Oxford (Blackwell).

Manuscript received: 30.01.2006

Accepted for publication: 05.04.2007